Article

SOURCE DATA | TRANSPARENT PROCESS | OPEN ACCESS

THE EMBO JOURNAL

MST2 methylation by PRMT5 inhibits Hippo signaling and promotes pancreatic cancer progression

Yan Sun[1,2,†], Xin Jin[3,4,†], Junpeng Meng[1,2,5], Feng Guo[1,2], Taoyu Chen[1,2], Xiaoyan Zhao[6,*], Heshui Wu[1,2,**] & Dianyun Ren[1,2,***]

Abstract

The Hippo signaling axis is a tumor suppressor pathway that is activated by various extra-pathway factors to regulate cell differentiation and organ development. Recent studies have reported that autophosphorylation of the core kinase cassette stimulates activation of the Hippo signaling cascade. Here, we demonstrate that protein arginine methyltransferase 5 (PRMT5) contributes to inactivation of the Hippo signaling pathway in pancreatic cancer. We show that the Hippo pathway initiator serine/threonine kinase 3 (STK3, also known as MST2) of Hippo signaling pathway can be symmetrically di-methylated by PRMT5 at arginine-461 (R461) and arginine-467 (R467) in its SARAH domain. Methylation suppresses MST2 autophosphorylation and kinase activity by blocking its homodimerization, thereby inactivating Hippo signaling pathway in pancreatic cancer. Moreover, we also show that the specific PRMT5 inhibitor GSK3326595 re-activates the dysregulated Hippo signaling pathway and inhibits the growth of human pancreatic cancer xenografts in immunodeficient mice, thus suggesting potential clinical application of PRMT5 inhibitors in pancreatic cancer.

Keywords dimerization; methylation; MST2; pancreatic cancer; PRMT5
Subject Categories Cancer; Post-translational Modifications & Proteolysis; Signal Transduction
DOI 10.15252/embj.2023114558 | Received 19 May 2023 | Revised 12 October 2023 | Accepted 16 October 2023 | Published online 31 October 2023
The EMBO Journal (2023) 42: e114558

Introduction

The Hippo signaling pathway was first identified from *Drosophila melanogaster* by the genetic screening, which was an evolutionarily highly conserved kinase-mediated signaling cascade to regulate cell proliferation and differentiation (Kim *et al*, 2022). The core components of classical Hippo pathway consist of the serine/threonine kinases mammalian Ste-20-like kinase 1/2 (MST1/2, Hippo in Drosophila) and large tumor suppressor 1/2 (LATS1/2), their scaffold proteins Salvador homolog 1 (SAV1) and Mps one binder 1 (MOB1), and the transcriptional co-activators YAP/TAZ (Jin *et al*, 2022). Especially, MST1/2, the initiators of Hippo signaling pathway, can form homodimers through their SARAH domains, and then autophosphorylate for activation (Ni *et al*, 2013; Tran *et al*, 2020) to phosphorylate MOB1 at threonine-12 (T12) and threonine-35 (T35) (Praskova *et al*, 2008), LATS1/2 at the hydrophobic motif (HM) with the help of binding partner SAV1 (Hergovich *et al*, 2006; Yin *et al*, 2013). Next, activated LATS1/2 promote YAP/TAZ phosphorylation to decrease YAP/TAZ nuclear translocation and promote their ubiquitination for degradation, thereby suppressing the transcriptional expression of downstream target genes (Karchugina *et al*, 2021). Therefore, the regulation of MST1/2 activity, including homodimers formation and autophosphorylation levels, is crucial for the initiation of Hippo signaling pathway.

Major advances have been made in the study of pancreatic ductal adenocarcinoma (PDAC) in recent years. However, PDAC remains one of the most lethal types of cancer because of the asymptomatic nature of the disease and lack of curative treatment modalities, with an overall 5-year survival rate of only about 7–8% (Wei *et al*, 2020; Hayashi *et al*, 2021). PDAC usually evolves resistance to conventional chemotherapy or targeted therapy, so it is necessary to explore a new treatment modality to improve the prognosis of PDAC patients. The major downstream effectors YAP/TAZ of Hippo pathway are increasingly recognized as a vital oncogene and their abundance and activity are elevated observably in many types of cancers, including PDAC (Moroishi *et al*, 2015; Mao *et al*, 2021). YAP exerts strong carcinogenic effects in multiple aspects of PDAC. YAP regulates the transcription of metabolic genes and metabolic

1 Department of Pancreatic Surgery, Union Hospital, Tongji Medical College, Huazhong University of Science and Technology, Wuhan, China
2 Sino-German Laboratory of Personalized Medicine for Pancreatic Cancer, Union Hospital, Tongji Medical College, Huazhong University of Science and Technology, Wuhan, China
3 Department of Urology, The Second Xiangya Hospital, Central South University, Changsha, China
4 Uro-Oncology Institute of Central South University, Changsha, China
5 Department of General Surgery, The Second Hospital of Shanxi Medical University, Taiyuan, China
6 Department of Hematology, Union Hospital, Tongji Medical College, Huazhong University of Science and Technology, Wuhan, China
*Corresponding author. Tel: +86 15534091397; E-mail: zxy2021@hust.edu.cn
**Corresponding author. Tel: +86 13720117761; E-mail: heshuiwu@hust.edu.cn
***Corresponding author. Tel: +86 13720290718; E-mail: rendianyun@hust.edu.cn
†These authors contributed equally to this work

reprogramming by transcribing MYC and cooperating with MYC in KRAS-driven PDAC (Murakami *et al*, 2019). YAP induces the differentiation and infiltration of myeloid-derived suppressor cells (MDSCs) to cause immunosuppressive microenvironment in PDAC (Murakami *et al*, 2017). Besides, YAP/TAZ activation drives tumor growth, metastasis and confers resistance to chemotherapy, immunotherapy, targeted therapy (Thompson, 2020). Importantly, the upstream Hippo signaling of YAP/TAZ identified as tumor suppressors frequently inactivates in many tumors, including PDAC (Yu *et al*, 2015; Ansari *et al*, 2019; Hayashi *et al*, 2021), which fails to inhibit the carcinogenic effects of YAP/TAZ. Therefore, restoring the upstream Hippo signaling of YAP/TAZ is significant for suppressing YAP/TAZ activation and PDAC progression.

As a widespread and classical post-translational modification (PTM), Protein arginine methylation participates in various cellular processes, including cell proliferation and differentiation, cellular metabolism, signal transduction, protein degradation and localization, etc (Blanc & Richard, 2017; Xu & Richard, 2021). Arginine methylation is catalyzed by protein arginine methyltransferases (PRMTs), which catalyze the transfer of a methyl group from S-adenosylmethionine (SAM) to the guanidino nitrogen atoms of arginine (Bedford & Clarke, 2009). Nine PRMTs have so far been identified in mammals and they are classified into three categories according to the catalytic type, type I (PRMT1-4, 6, 8) for catalyzing mono-methylarginine (MMA/α-me1) and asymmetric di-methylarginine (ADMA/α-me2a), type II (PRMT5, 7, 9) for catalyzing me1 and symmetric di-methylarginine (SDMA/α-me2s), type III (PRMT7) for catalyzing mono-methylation reactions of certain substrates (Yang & Bedford, 2013; Wang *et al*, 2016). Recent evidences indicate that PRMT5 overexpression leads to the worse survival and inhibition of PRMT5 slows PDAC progression (Berglund *et al*, 2008; Lee *et al*, 2021), and PRMT5 silencing improves PDAC sensitivity to multiple drugs, such as Gemcitabine (Wei *et al*, 2020) and Palbociclib (AbuHammad *et al*, 2019), which suggests that PRMT5 is an emerging target for PDAC patients. Thus, further in-depth exploration of PRMT5 functions in PDAC is of great significance for improving PDAC prognosis.

Emerging evidences suggested that PRMT5 participated in inducing the inactivation of Hippo signaling pathway in PDAC. We found that the initiator MST2 of Hippo pathway could be methylated at arginine-461 (R461) and arginine-467 (R467) in SARAH domain by PRMT5. The methylated MST2 was unable to form homodimers through the SARAH domain, thereby failed to autophosphorylate for activation, which caused the inactivation of Hippo signaling pathway in PDAC. Thus, MST2 methylation was closely related to inactivated Hippo signaling pathway and progressive PDAC.

Results

PRMT5 induces the inactivation of Hippo signaling pathway in PDAC

The increased PRMT5 expression occurs in a variety of tumors including PDAC, which causes tumor progression and poor prognosis (Lee *et al*, 2021). Although some studies related to PRMT5 have been carried out in PDAC, its tumor-promoting mechanism in PDAC remains unclear. To further explore the mechanism, RNA-seq was conducted after pancreatic cancer cells were treated with PRMT5 inhibitor GSK3326595. The results showed that inhibiting PRMT5 activity reduced the levels of downstream genes of YAP1 (Fig 1A). Four of the genes were verified by qRT–PCR and immunoblotting and the results were consistent with RNA-seq (Fig 1B and C). Then we constructed PRMT5 KO pancreatic cancer cells, and PRMT5 WT and PRMT5 G367A/R368A enzymatic-dead mutant were respectively re-introduced into the cells of PRMT5 KO to detect the changes of Hippo pathway and its downstream genes (Fig EV1A–C). The results showed that the levels of CYR61/CTGF/AURKB/ANKRD1 were obviously decreased after PRMT5 was knocked out (Figs 1D and F, and EV1D and E), while re-introduced PRMT5 WT but not PRMT5 G367A/R368A mutant restored the expression of four genes (Figs 1E and G, and EV1F and G). Importantly, the results also showed the up-regulated pLATS1-Ser909 and pLATS1-Thr1079 level, pYAP1-Ser127 and pYAP1-Ser397 level, as well as down-regulated YAP1 expression after PRMT5 was knocked out (Figs 1F and EV1E), but the decreased pLATS1-Ser909 and pLATS1-Thr1079 level, pYAP1-Ser127 and pYAP1-Ser397 level, as well as increased YAP1 expression were observed when PRMT5 WT instead of PRMT5 G367A/R368A mutant was re-expressed in PRMT5 KO cells (Figs 1G and EV1G). These data indicated that PRMT5 inhibited the phosphorylation cascade of the Hippo signaling pathway through its arginine methyltransferase activity. Moreover, the change of effector YAP1 was also monitored. Subcellular fractionation and immunofluorescence assays showed that PRMT5 deletion retained more YAP1 in the cytoplasm (Fig 1H–J), whereas PRMT5 WT but not PRMT5 G367A/R368A mutant promoted more YAP1 to enter the cell nucleus (Fig 1K–M). YAP1 residing in the cytoplasm was also further ubiquitinated and degraded after PRMT5 deletion (Fig EV1H), and PRMT5 WT but not G367A/R368A mutant reduced YAP1 ubiquitination to keep YAP1 protein stable (Fig EV1I). In summary, PRMT5 inactivates the Hippo signaling pathway through its arginine methyltransferase activity.

MST2 is di-methylated symmetrically at R461 and R467 in the C-terminal SARAH domain

Given that PRMT5 induced the inactivation of Hippo pathway by its enzymatic activity, SDMA-shotgun was performed to find the related mechanisms. Surprisingly, MST2 (also known as STK3) appeared to be di-methylated symmetrically (Fig 2A). To confirm the results of SDMA-shotgun, endogenous MST2 was detected with the anti-α-me2s antibody (CST). The results showed that human MST2 was indeed di-methylated symmetrically and the SDMA level was decreased after treatment with the nonspecific PRMT inhibitor adenosine dialdehyde (AdOx), and the reduction effect was more and more obvious along with the incremental AdOx concentration and treatment time (Fig 2B). Similarly, the purified exogenous Flag-MST2 was also di-methylated symmetrically and AdOx remarkably reduced the SDMA level whether in pancreatic cancer cells or HEK293T cells, also accompanied with AdOx concentration dependence and AdOx time dependence (Fig 2C and D). The SDMA-shotgun hinted that MST2 was di-methylated symmetrically at R461 and R467 (Fig 2A and E), and multiple sequence alignments from various species also showed that R461 was a highly conserved amino acid residue and R467 was a relatively conserved amino acid residue (Fig 2F and G). Therefore, R461 and R467 might be the potential methylated sites. To prove the conjecture, R461 and R467

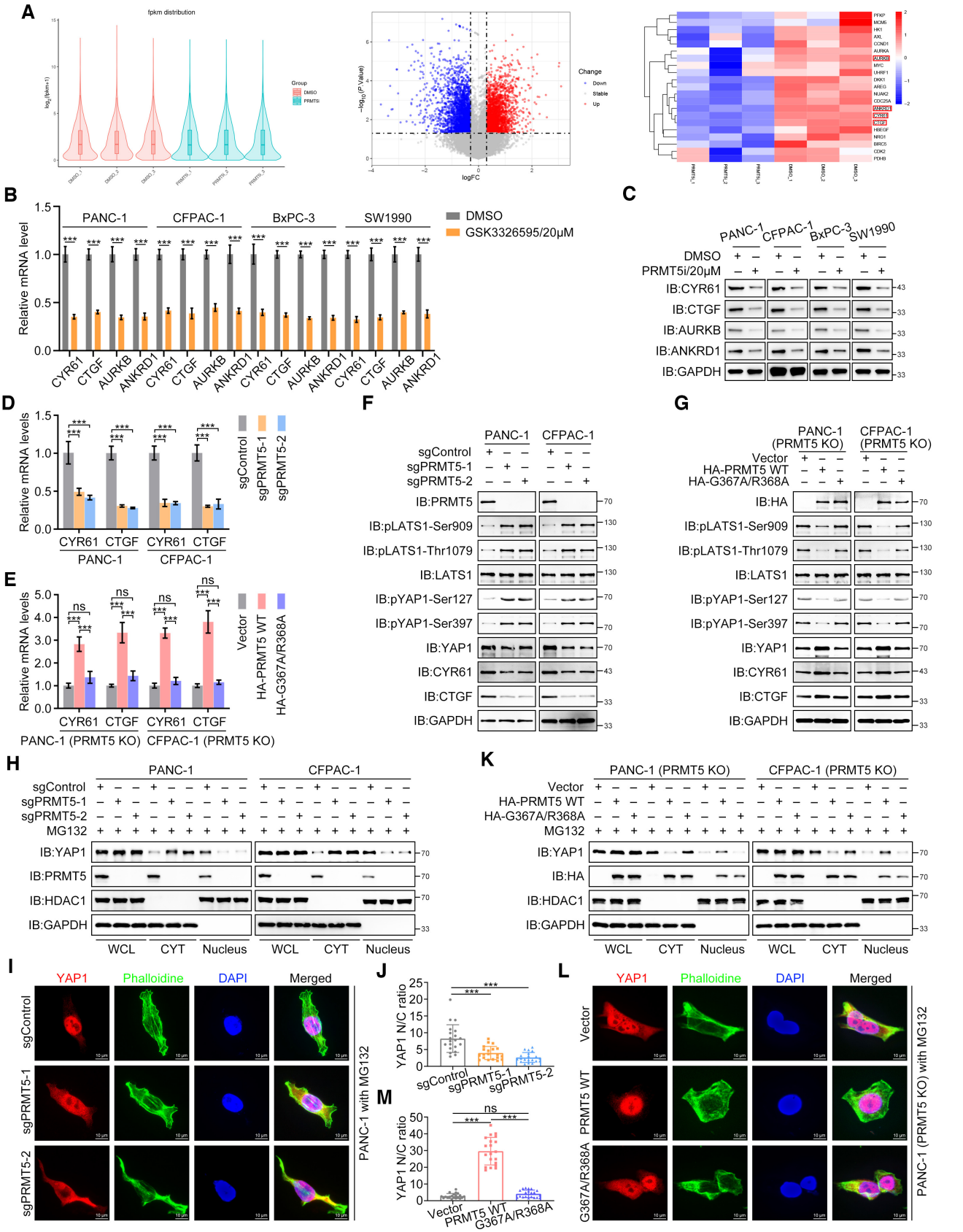
A
fpkm distribution
Group
DMSO
PRMT5i
Change
Down
Stable
Up
logFC
B
PANC-1
CFPAC-1
BxPC-3
SW1990
DMSO
GSK3326595/20μM
Relative mRNA level
CYR61
CTGF
AURKB
ANKRD1
C
DMSO
PRMT5i/20μM
IB:CYR61
IB:CTGF
IB:AURKB
IB:ANKRD1
IB:GAPDH
D
Relative mRNA levels
sgControl
sgPRMT5-1
sgPRMT5-2
PANC-1
CFPAC-1
E
Vector
HA-PRMT5 WT
HA-G367A/R368A
PANC-1 (PRMT5 KO)
CFPAC-1 (PRMT5 KO)
F
IB:PRMT5
IB:pLATS1-Ser909
IB:pLATS1-Thr1079
IB:LATS1
IB:pYAP1-Ser127
IB:pYAP1-Ser397
IB:YAP1
G
H
MG132
IB:HDAC1
WCL
CYT
Nucleus
K
I
YAP1
Phalloidine
DAPI
Merged
PANC-1 with MG132
J
YAP1 N/C ratio
M
L
PANC-1 (PRMT5 KO) with MG132

Figure 1.

Figure 1. PRMT5 induces the inactivation of Hippo signaling pathway in PDAC.

A The boxplot showed the distribution of gene expression levels in different samples after calculating the FPKM values. The abscissa was the sample name and the ordinate is $\log_2$(FPKM+1). From top to bottom, each box represented the maximum value, upper quartile (75%), median, lower quartile (25%), and minimum value of gene expression. The width of each violin represented the number of genes at the indicated expression level. YAP1 downstream genes were plotted as the heatmap based on the RNA-Seq of BxPC-3 after GSK3326595 treatment. The differentially expressed genes were analyzed by DESeq2 and *P*-values were calculated by negative binomial distribution. Then multiple hypothesis testing was performed by Benjamini–Hochberg to obtain FDR-values. Each treatment group had three biological replicates ($n = 3$).

B, C Pancreatic cancer cells were treated with 20 μM GSK3326595. The cells were harvested for qRT–PCR after 48 h (B) and immunoblotting after 72 h (C). Data were shown as mean ± SD ($n = 3$ biological replicates). ***$P < 0.001$. The statistical significance was tested by the two-way ANOVA. Immunoblotting analysis was repeated biologically three times independently.

D, E PANC-1 and CFPAC-1 cells were extracted RNA for qRT–PCR after PRMT5 was knocked out (D) or PRMT5 WT/mutant was re-expressed (E). Data were shown as mean ± SD ($n = 3$ biological replicates). ns, not significant; ***$P < 0.001$. The statistical significance was tested by the two-way ANOVA.

F, G PANC-1 and CFPAC-1 were used to detect the change of Hippo components by immunoblotting after PRMT5 was knocked out (F) or PRMT5 WT/mutant was re-expressed (G). Immunoblotting analysis was repeated three times independently.

H–J PRMT5-KO cells were treated with 10 μM MG132 for 72 h. Nucleocytoplasmic separation was performed to detect the localization of YAP1 (H). And the MG132-treated PRMT5-KO PANC-1 cells were transferred to the cell culture slides for immunofluorescence. The representative images (I) and the quantification (J) of 20 cells were shown in the figure. Scale bar: 10 μm. Immunoblotting analysis was repeated three times independently. The statistical significance was tested by the one-way ANOVA (J). ***$P < 0.001$. Data were shown as mean ± SD ($n = 20$ biological replicates).

K–M PRMT5-KO cells were re-expressed HA-PRMT5 WT or G367A/R368A. Then, the cells were treated with 10 μM MG132 for 72 h. Nucleocytoplasmic separation was performed to detect the localization of YAP1 (K). And the above PANC-1 cells were transferred to the cell culture slides for immunofluorescence. The representative images (L) and the quantification (M) of 20 cells were shown in the figure. Scale bar: 10 μm. Immunoblotting analysis was repeated three times independently. The statistical significance was tested by the one-way ANOVA (M). ns, not significant; ***$P < 0.001$. Data were shown as mean ± SD ($n = 20$ biological replicates).

Source data are available online for this figure.

were replaced with lysine (K), individually or in combination in Flag-MST2 (Fig 2H). The results showed that individually mutating each R site markedly interfered the SDMA level of MST2, and SDMA was fully eliminated after both sites were mutated (Fig 2I). The α-me2s antibody from Antibodies-online was also validated, which could be used for immunoblotting (Fig EV2A). Moreover, both MST2 wild type (WT) and single R-to-K mutant (R461K or R467K) displayed the discernible response in SDMA, while the SDMA level of 2RK mutant (R461/467K) completely abolished symmetric dimethylation did not change after AdOx treatment in pancreatic cancer cells and HEK293T cells, which further verified that MST2 was di-methylated symmetrically at R461 and R467 (Fig EV2B–E). Together, MST2 is di-methylated symmetrically at R461 and R467 in the C-terminal SARAH domain in pancreatic cancer cells.

PRMT5 catalyzes the symmetric dimethylation of MST2 at R461 and R467

SDMA of MST2 suggested type II PRMTs were responsible for the modification. To identify the PRMTs, Flag-MST2 were transfected into pancreatic cancer cells for Co-IP assay. The results showed only PRMT5, not PRMT7 and PRMT9, could be co-precipitated by Flag-MST2 (Fig EV3A). Further research found the key chaperone protein MEP50 that maintained PRMT5 enzymatic activity (Stopa *et al*, 2015) was also co-precipitated by Flag-MST2 (Fig 3A). And the interactions could be detected between any two of the three proteins (Figs 3A and B, and EV3B). These data implied that PRMT5 might be the arginine methyltransferase of MST2. To prove this possible inference, PRMT5, PRMT7 and PRMT9 were respectively deleted in pancreatic cancer cells, and the results showed that PRMT5-KO significantly decreased the SDMA level of MST2 (Fig 3C) while PRMT7-KO and PRMT9-KO had no effect (Fig EV3C and D). Similarly, GSK3326595 also suppressed the SDMA level of MST2 in a concentration- and time-dependent manner as did AdOx (Figs 3D and EV3E). Moreover, both overexpressed PRMT5 and MEP50 up-regulated the SDMA level of MST2 and their combination further enhanced the effect (Fig 3E), but increased PRMT7 and PRMT9 expression failed to promote MST2 methylation (Fig EV3F). These results suggested that PRMT5 was the arginine methyltransferase of MST2. Subsequently, we found that SDMA of MST2 could be redetected only after restoring PRMT5 expression in PRMT5-KO cells (Fig 3F), and reintroduction of PRMT5 WT rescued MST2 methylation rather than G367A/R368A mutant (Fig 3G), which further demonstrated MST2 was a bona fide substrate of PRMT5. Furthermore, PRMT5 failed to catalyze MST2 methylation after R-to-K conversion (Fig 3H) and low-methylated MST2 caused by RK mutations gradually reduced its response to PRMT5 inhibitor until no response after complete demethylation (Fig EV3G and H). Most importantly, *in vitro* methylation assay illustrated that wild-type arginine in MST2 and enzymatic activity in PRMT5 were indispensable for the methylation reaction (Fig 3I). These data indicated that PRMT5 di-methylates symmetrically MST2 at R461 and R467. The above researches showed MST2 bound to PRMT5, so we next wondered whether MST2 directly bound to PRMT5 and which region interacted with PRMT5. We constructed recombinant full-length GST-tagged MST2 and truncated GST-MST2 for GST pull-down (Fig 3J). The results showed that the untruncated GST-MST2 directly bound to PRMT5 and the deletion of SARAH domain eliminated the interaction (Fig 3K). And MST2 lacking the SARAH domain could also no longer be symmetrically di-methylated (Fig 3L), indicating the SARAH domain of MST2 was indispensable in the methylation reaction. Moreover, the weak downregulation of MST2 SDMA was also observed after 4 h of treatment with GSK3326595 and the SDMA level decreased rapidly along with the increase of GSK3326595 treatment time, which suggested that the SDMA of MST2 could be rapidly eliminated by PRMT5 inhibitor (Fig 3M). We also further explored the effects of external stimuli on MST2 SDMA, which showed high glucose (HG) environment promoted MST2 SDMA and hydrogen peroxide-induced oxidative stress reduced the SDMA level of MST2 (Fig 3N and O). Additionally, we also examined whether

MST1 (a homolog of MST2) could be methylated by PRMT5. The results showed that Q457 and R463 of MST1 corresponding to R461 and R467 of MST2 were highly conserved (Fig EV3I and J), but MST1 could only bound indirectly to PRMT5 through MST2 and MST1 failed to be di-methylated symmetrically (Fig EV3K–M).

The SDMA of MST2 inhibits the activation of Hippo signaling pathway

As the central component of the Hippo signaling pathway, the phosphorylation and activation of kinase MST2 play a vital role of

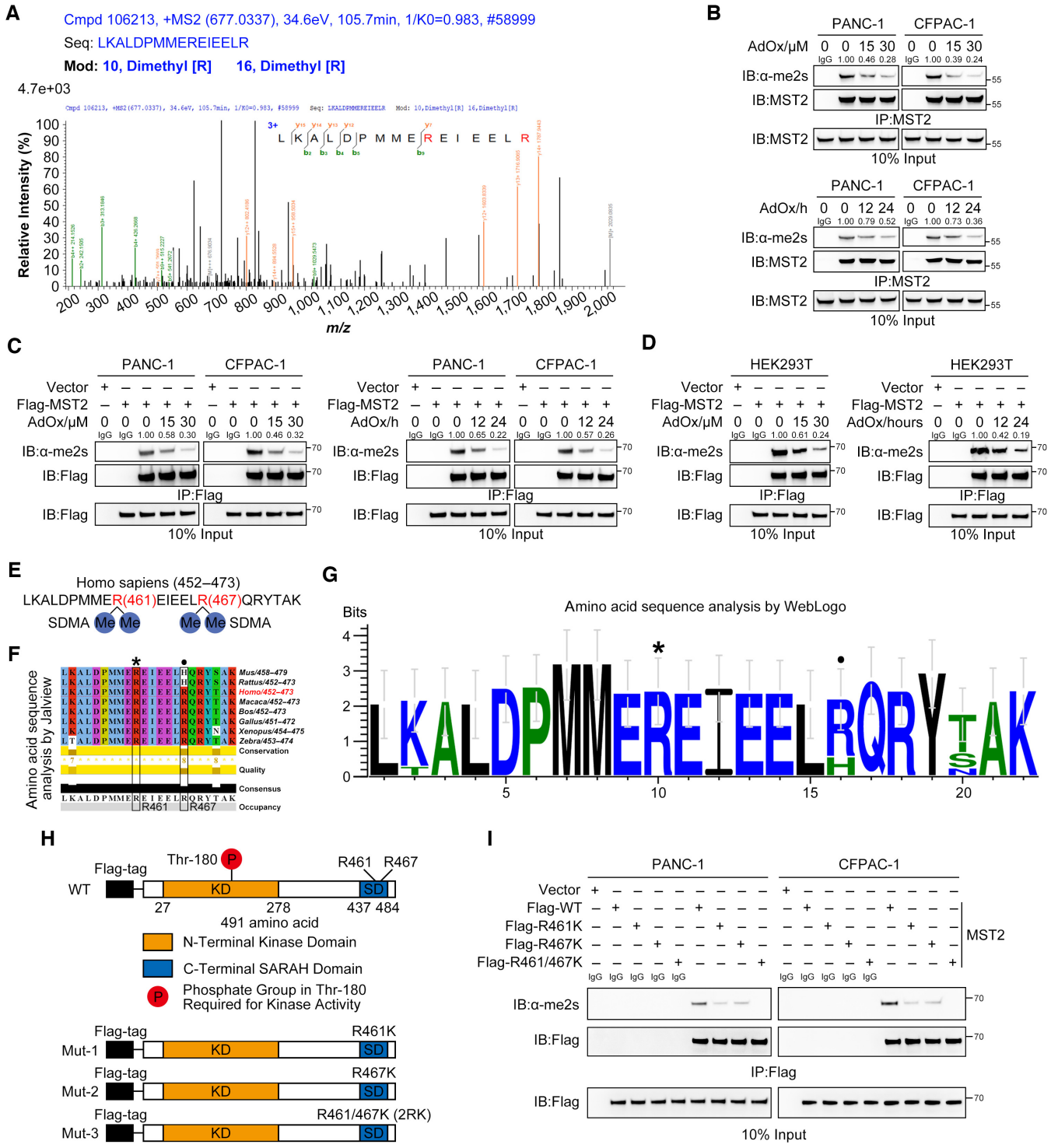

Figure 2.

Figure 2. MST2 is di-methylated symmetrically at R461 and R467 in the C-terminal SARAH domain.

A The SDMA sites of MST2 were initially identified by SDMA-shotgun analysis.
B PANC-1 and CFPAC-1 were treated with AdOx in an increasing concentration gradient manner for 24 h or an increasing time gradient manner with 30 μM. Then, endogenous MST2 was precipitated to detect the SDMA. Immunoblotting analysis was repeated three times independently.
C, D PANC-1, CFPAC-1, and HEK293T were treated with AdOx by the above method after overexpressing Flag-MST2. Then, the immunopurified Flag-MST2 was detected with anti-α-me2s antibody. Immunoblotting analysis was repeated three times independently.
E The sketch map was drawn to describe the SDMA sites of MST2.
F, G Multiple sequence alignments of MST2 amino acid were performed in various species by Jalview (F) and visualized by WebLogo (G).
H The schematic showed that arginine (R) was mutated into lysine (K) on Flag-MST2.
I PANC-1 and CFPAC-1 were transfected with the indicated plasmids. After 72 h, Flag-MST2 was precipitated by anti-Flag magnetic beads to detect the SDMA. Immunoblotting analysis was repeated three times independently.

Source data are available online for this figure.

initiator to stimulate the activation of the entire Hippo signaling pathway (Fan *et al*, 2016; Tran *et al*, 2020). To investigate whether SDMA affected the regulating effect of MST2 on the Hippo signaling pathway, we constructed MST2 KO pancreatic cancer cells to eliminate endogenous MST2 interference (Fig EV4A). Then exogenous Flag-MST2 WT, R461K, R467K and R461/467K was re-expressed separately in MST2 KO cells to detect the change of Hippo signaling pathway (Fig 4A). The results showed the expression of CYR61 and CTGF was increased after MST2 was knocked out (Fig EV4B and C), while re-expressed Flag-MST2 WT and mutant suppressed the expression of CYR61 and CTGF, and 2RK mutant displayed the strong inhibitory effect, R461K or R467K came second and WT was the weakest (Fig 4B and C). More importantly, we discovered the decreased LATS1 phosphorylation at Ser909 and Thr1079, YAP1 phosphorylation at Ser127 and Ser397, and increased YAP1 level when MST2 was knocked out (Fig EV4C), but the progressively incremental LATS1 phosphorylation at Ser909 and Thr1079, YAP1 phosphorylation at Ser127 and Ser397, and progressively diminishing YAP1 level after respectively re-expressing Flag-MST2 WT, single RK mutant, 2RK mutant (Fig 4C). Subsequently, we also observed MST2 deletion caused more YAP1 to enter the cell nucleus (Fig EV4D–F) and lower YAP1 ubiquitination level to maintain stability (Fig EV4G), whereas Flag-MST2 WT, single RK mutant, 2RK mutant gradually promoted increasing YAP1 in the cytoplasm (Fig 4D–F) and increasing YAP1 ubiquitination level for degradation (Fig 4G). Besides, MST2 deletion not only led to the proliferation of pancreatic cancer cells *in vitro* (Fig EV4H–J) but also promoted the progression of pancreatic cancer in mice (Fig EV4K–M). Nevertheless, re-expressed exogenous Flag-MST2 reversed the hyperproliferation of pancreatic cancer cells caused by MST2 KO, and the inhibitory effect on cell proliferation became stronger and stronger along with the increasing R-to-K mutations in MST2 (Fig 4H–J). And the exogenous Flag-MST2 also slowed the progression of pancreatic cancer in mice, which had an increasingly pronounced effect along with an increase in the number of MST2 R-to-K mutations (Fig 4K–M). In conclusion, these data indicated that SDMA of MST2 suppresses the activation of the Hippo signaling pathway.

SDMA suppresses MST2 autophosphorylation and kinase activity by decreasing the level of MST2 homodimer

So what mechanism does MST2 SDMA suppress the Hippo pathway? It is known that MST2 phosphorylation at Thr180 on the activation loop, primarily attributed to the trans-autophosphorylation of MST2, is required for MST2 kinase activity (Praskova *et al*, 2004; Deng *et al*, 2013; Tran *et al*, 2020). Our study suggested that MST2 was indeed autophosphorylated in the presence of both MST2-Thr180 and kinase activity (Fig EV5A–C). A series of evidences also suggest that MST2 autophosphorylation depends on homodimerization mediated by its SARAH domain (Creasy *et al*, 1996; Jin *et al*, 2012; Bae & Luo, 2018; Tran *et al*, 2020). And R461 and R467 were exactly located in the SARAH domain of MST2. Therefore, we speculated that SDMA affected MST2 autophosphorylation and kinase activity by interfering with homodimerization (Fig 5A). To verify this ratiocination, the interactional intensity between Flag-tagged MST2 and GFP-tagged MST2 was detected by co-immunoprecipitation (Co-IP) assay. Unsurprisingly, 2RK mutant significantly enhanced the binding between Flag-MST2 and GFP-MST2 compared to R461K mutant and R467K mutant, while Flag-MST2 WT showed the weaker binding than single RK mutants (Fig 5B). The endogenous MST2 precipitated by exogenous GFP-MST2 also showed the consistent results in pancreatic cancer cells (Fig 5C). Moreover, glutaraldehyde cross-linking assays also showed that MST2 gradually converted from monomer to homodimer along with the increasing R-to-K mutations (Fig 5D), and SDMA was only detected in the monomeric form of Flag-MST2 WT (high SDMA level) and single RK mutant (low SDMA level) rather than 2RK mutant and the dimeric form (Fig 5E). As mentioned above, MST2 homodimerization promotes its autophosphorylation, thus we tested the effect of SDMA on MST2 autophosphorylation. As expected, the level of MST2 autophosphorylation at Thr180 was gradually increased with the increasing number of RK mutations (Fig 5F). Besides, *in vitro* kinase assay also showed that the level of MST2 autophosphorylation was higher if MST2 SDMA was continuously reduced (Fig 5G). Furthermore, MST2 kinase activity was also measured to evaluate the effect of SDMA on kinase activity, which showed that RK mutants enhanced the kinase activity of MST2 (Fig 5H). Additionally, the SARAH domain was responsible for homodimerization and heterodimerization as well as binding to additional proteins that lack this domain (Karchugina *et al*, 2021), so we also examined the interaction of MST2-methylation deleted mutants with MST1/SAV1/LATS1, which showed that the strength of interaction was enhanced after MST2 demethylation (Fig EV5D–F). Given that PRMT5 catalyzed MST2 SDMA, GSK3326595 was also used to further verify the above results in pancreatic cancer cells. We first explored the sensitivity of pancreatic cancer cells to GSK3326595. One study showed that GSK3326595 of 250 nM/500 nM was sufficient to inhibit the arginine methyltransferase activity of PRMT5 in human melanoma cell lines HT144/A375, but required 6 days of treatment (AbuHammad *et al*, 2019). Our results

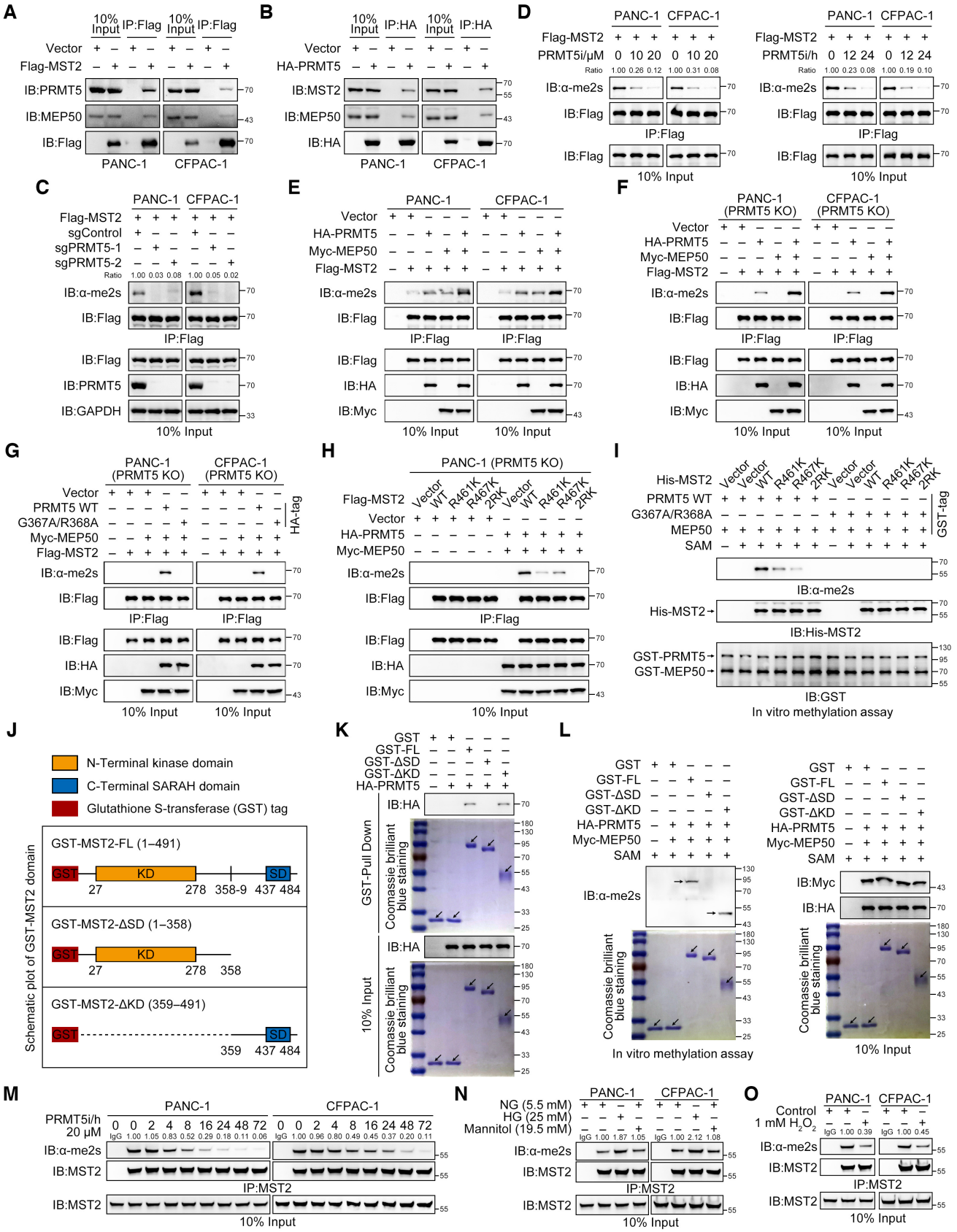
A
10% Input IP:Flag 10% Input IP:Flag
Vector + – + – + – + –
Flag-MST2 – + – + – + – +
IB:PRMT5
IB:MEP50
IB:Flag
PANC-1 CFPAC-1
B
10% Input IP:HA 10% Input IP:HA
Vector + – + – + – + –
HA-PRMT5 – + – + – + – +
IB:MST2
IB:MEP50
IB:HA
PANC-1 CFPAC-1
D
PANC-1 CFPAC-1
Flag-MST2 + + + + + +
PRMT5i/μM 0 10 20 0 10 20
Ratio 1.00 0.26 0.12 1.00 0.31 0.08
IB:α-me2s
IB:Flag
IP:Flag
IB:Flag
10% Input
PANC-1 CFPAC-1
Flag-MST2 + + + + + +
PRMT5i/h 0 12 24 0 12 24
Ratio 1.00 0.23 0.08 1.00 0.19 0.10
IB:α-me2s
IB:Flag
IP:Flag
IB:Flag
10% Input
C
PANC-1 CFPAC-1
Flag-MST2 + + + + + +
sgControl + – – + – –
sgPRMT5-1 – + – – + –
sgPRMT5-2 – – + – – +
Ratio 1.00 0.03 0.08 1.00 0.05 0.02
IB:α-me2s
IB:Flag
IP:Flag
IB:Flag
IB:PRMT5
IB:GAPDH
10% Input
E
PANC-1 CFPAC-1
Vector + + – – – + + – – –
HA-PRMT5 – – + – + – – + – +
Myc-MEP50 – – – + + – – – + +
Flag-MST2 – + + + + – + + + +
IB:α-me2s
IB:Flag
IP:Flag IP:Flag
IB:Flag
IB:HA
IB:Myc
10% Input 10% Input
F
PANC-1 (PRMT5 KO) CFPAC-1 (PRMT5 KO)
Vector + + – – – + + – – –
HA-PRMT5 – – + – + – – + – +
Myc-MEP50 – – – + + – – – + +
Flag-MST2 – + + + + – + + + +
IB:α-me2s
IB:Flag
IP:Flag IP:Flag
IB:Flag
IB:HA
IB:Myc
10% Input 10% Input
G
PANC-1 (PRMT5 KO) CFPAC-1 (PRMT5 KO)
Vector + + + – – + + + – –
PRMT5 WT – – – + – – – – + –
G367A/R368A – – – – + – – – – +
Myc-MEP50 – – + + + – – + + +
Flag-MST2 – + + + + – + + + +
HA-tag
IB:α-me2s
IB:Flag
IP:Flag IP:Flag
IB:Flag
IB:HA
IB:Myc
10% Input 10% Input
H
PANC-1 (PRMT5 KO)
Flag-MST2 Vector WT R461K R467K 2RK Vector WT R461K R467K 2RK
Vector + + + + + – – – – –
HA-PRMT5 – – – – – + + + + +
Myc-MEP50 – – – – - + + + + +
IB:α-me2s
IB:Flag
IP:Flag
IB:Flag
IB:HA
IB:Myc
10% Input
I
His-MST2 Vector Vector WT R461K R467K 2RK Vector Vector WT R461K R467K 2RK
PRMT5 WT + + + + + + – – – – – –
G367A/R368A – – – – – – + + + + + +
MEP50 + + + + + + + + + + + +
SAM – + + + + + – + + + + +
GST-tag
IB:α-me2s
His-MST2
IB:His-MST2
GST-PRMT5
GST-MEP50
IB:GST
In vitro methylation assay
J
N-Terminal kinase domain
C-Terminal SARAH domain
Glutathione S-transferase (GST) tag
Schematic plot of GST-MST2 domain
GST-MST2-FL (1–491)
GST KD SD
27 278 358-9 437 484
GST-MST2-ΔSD (1–358)
GST KD
27 278 358
GST-MST2-ΔKD (359–491)
GST SD
359 437 484
K
GST + + – – –
GST-FL – – + – –
GST-ΔSD – – – + –
GST-ΔKD – – – – +
HA-PRMT5 – + + + +
IB:HA
GST-Pull Down
Coomassie brilliant blue staining
IB:HA
10% Input
Coomassie brilliant blue staining
L
GST + + – – –
GST-FL – – + – –
GST-ΔSD – – – + –
GST-ΔKD – – – – +
HA-PRMT5 – + + + +
Myc-MEP50 – + + + +
SAM + + + + +
IB:α-me2s
Coomassie brilliant blue staining
In vitro methylation assay
GST + + – – –
GST-FL – – + – –
GST-ΔSD – – – + –
GST-ΔKD – – – – +
HA-PRMT5 – + + + +
Myc-MEP50 – + + + +
SAM + + + + +
IB:Myc
IB:HA
Coomassie brilliant blue staining
10% Input
M
PANC-1 CFPAC-1
PRMT5i/h 0 0 2 4 8 16 24 48 72 0 0 2 4 8 16 24 48 72
20 μM IgG 1.00 1.05 0.83 0.52 0.29 0.18 0.11 0.06 IgG 1.00 0.96 0.80 0.49 0.45 0.37 0.20 0.11
IB:α-me2s
IB:MST2
IP:MST2
IB:MST2
10% Input
N
PANC-1 CFPAC-1
NG (5.5 mM) + + + + + – – – – –
HG (25 mM) – – – + – – – – + –
Mannitol (19.5 mM) – – – – + – – – – +
IgG 1.00 1.87 1.05 IgG 1.00 2.12 1.08
IB:α-me2s
IB:MST2
IP:MST2
IB:MST2
10% Input
O
PANC-1 CFPAC-1
Control + + – + + –
1 mM H_2O_2 – – + – – +
IgG 1.00 0.39 IgG 1.00 0.45
IB:α-me2s
IB:MST2
IP:MST2
IB:MST2
10% Input

Figure 3.

Figure 3. PRMT5 catalyzes the symmetric dimethylation of MST2 at R461 and R467.

A PANC-1 and CFPAC-1 were transfected with Flag-MST2 for 72 h. Then, PRMT5 and MEP50 co-precipitated by Flag-MST2 were detected by Co-IP. Immunoblotting analysis was repeated three times independently.

B PANC-1 and CFPAC-1 were transfected with HA-PRMT5 for 72 h. Then, MST2 and MEP50 co-precipitated by HA-PRMT5 were detected by Co-IP. Immunoblotting analysis was repeated three times independently.

C PRMT5-KO cells were transfected with Flag-MST2. Then, Flag-MST2 was precipitated to detect the SDMA. Immunoblotting analysis was repeated three times independently.

D PANC-1 and CFPAC-1 expressed Flag-MST2 were treated with GSK3326595 in the increasing dosage manner for 24 h or the increasing time manner with 20 μM. Then Flag-MST2 was precipitated to detect the SDMA. Immunoblotting analysis was repeated three times independently.

E, F PANC-1 and CFPAC-1 were transfected with the indicated plasmids (E), so did PRMT5-KO cells (F). Then Flag-MST2 was precipitated to detect the SDMA. Immunoblotting analysis was repeated three times independently.

G, H PRMT5-KO cells were transfected with the indicated plasmids. Then, Flag-MST2 was precipitated to detect the SDMA. Immunoblotting analysis was repeated three times independently.

I Recombinant His-MST2 was expressed in *E. coli* BL21 and purified by His-tag Protein Purification Kit. Recombinant GST-PRMT5/MEP50 were transfected into HEK293T and purified by anti-GST magnetic beads. Then, His-MST2 was incubated with GST-PRMT5/MEP50 with or without 100 μM SAM. Immunoblotting analysis was repeated three times independently.

J The schematic described the constructed recombinant GST-MST2 proteins.

K Recombinant GST-MST2 was expressed in *E. coli* BL21 and GST-tagged proteins were purified by anti-GST magnetic beads. HA-PRMT5 plasmids were transfected into HEK293T and HA-tagged proteins were purified by anti-HA magnetic beads. Then, GST-MST2 was incubated with HA-PRMT5 for GST pull-down. Immunoblotting analysis was repeated three times independently. Arrows indicated the protein bands at the expected molecular weight.

L GST-MST2 was incubated with HA-PRMT5 in the presence of SAM *in vitro*. Immunoblotting analysis was repeated three times independently. Arrows indicated the protein bands at the expected molecular weight.

M PANC-1 and CFPAC-1 were treated with GSK3326595 and harvested at different time points to detect SDMA. Immunoblotting was repeated three times independently.

N, O The SDMA was detected after cells were treated with high glucose (N) or hydrogen peroxide (O). Immunoblotting was repeated three times independently.

Source data are available online for this figure.

showed 0.5 μM GSK3326595 for 24 h could hardly suppress PRMT5 activity, but the significant suppressive effects could be observed after treatment with 10 μM/20 μM GSK3326595, which suggested that high concentration of GSK3326595 could exert the inhibitory effect in a short time (Fig EV5G). Then the SDMA level of MST2 was detected to assess PRMT5 activity after pancreatic cancer cells were treated for 0/2/4/6 days with 500 nM GSK3326595. However, the results showed that 500 nM GSK3326595 for 6 days did not worked as well as had been hoped, which only mildly inhibited PRMT5 activity (Fig EV5H). Whereafter, low-dose GSK3326595 (100 and 500 nM) was also used to verify the results. Unsurprisingly, 500 nM GSK3326595 only weakly inhibited MST2 SDMA (Fig EV5I), in turn slightly increased the level of pMST2-Thr180 (Fig EV5I) and MST2 homodimerization (Fig EV5J). Therefore, the effect of 500 nM GSK3326595 on activating Hippo signaling pathway was also relatively limited (Fig EV5K and L). No changes were observed in the treatment group of lower-dose (100 nM) GSK3326595 (Fig EV5I–L). It can thus be seen that pancreatic cancer cells require a high-dose GSK3326595. Then the high-dose GSK3326595 was used to treat pancreatic cancer cells, which showed the enhanced binding in a dose-dependent and time-dependent manner between differently tagged MST2 (Fig 5I and J). In summary, SDMA decreases the level of MST2 homodimer, thereby suppressing MST2 autophosphorylation and kinase activity.

PRMT5 suppresses MST2 autophosphorylation and kinase activity by blocking symmetrical di-methylated MST2 homodimerization

Similar to pancreatic cancer cells, GSK3326595 also strengthened the binding between Flag-MST2 and GFP-MST2 in the dose-dependent and time-dependent manner in HEK293T cells (Fig 6A). While the re-introduce of PRMT5 WT but not G367A/R368A mutant significantly weakened the interaction in PRMT5-KO cells (Fig 6B). The precipitated endogenous MST2 by exogenous GFP-MST2 also showed the consistent trend after GSK3326595 treatment in pancreatic cancer cells (Fig 6C). We also discovered that PRMT5 WT instead of G367A/R368A mutant led to a noticeable dimer-to-monomer conversion by glutaraldehyde cross-linking assay (Fig 6D). In addition, neither inhibition nor overexpression of PRMT5 could modulate the interaction between Flag-MST2 and GFP-MST2 after MST2 was completely demethylated by 2R-to-2K mutations (Appendix Fig S1A and B). These data suggested that PRMT5 prevented the homodimerization of MST2 through its arginine methyltransferase activity. As mentioned earlier, the formation of MST2 homodimer was required for its autophosphorylation at Thr180, so we assessed the impact of PRMT5 on MST2 autophosphorylation and kinase activity. The results showed that the level of MST2 autophosphorylation at Thr180 was gradually incremental along with the increasing PRMT5 inhibitor concentration and extended treatment time (Fig 6E), and PRMT5 KO generated the same effect as GSK3326595 (Fig 6F). While the upregulated pMST2-Thr180 level in PRMT5 KO cells was re-suppressed by PRMT5 WT rather than G367A/R368A mutant (Fig 6G). Similarly, PRMT5 could no longer regulate MST2 autophosphorylation after MST2 WT was mutated into R461/467K (Appendix Fig S1C). What's more, MST2 kinase activity assay showed that the kinase activity of both endogenous and exogenous MST2 was enhanced after GSK3326595 treatment (Fig 6H and I). Simultaneously, PRMT5 KO up-regulated the kinase activity of MST2 and PRMT5 WT instead of G367A/R368A mutant down-regulated the kinase activity of MST2 (Fig 6J and K). These results highlighted the importance of PRMT5 for MST2 autophosphorylation and kinase activity. Additionally, the binding capacity of MST2 with MST1/SAV1/LATS1 was also detected, which showed that PRMT5-deletion enhanced the binding capacity (Appendix Fig S1D). GSK3326595 treatment also showed the consistent results (Appendix Fig S1E). In conclusion, our studies indicated

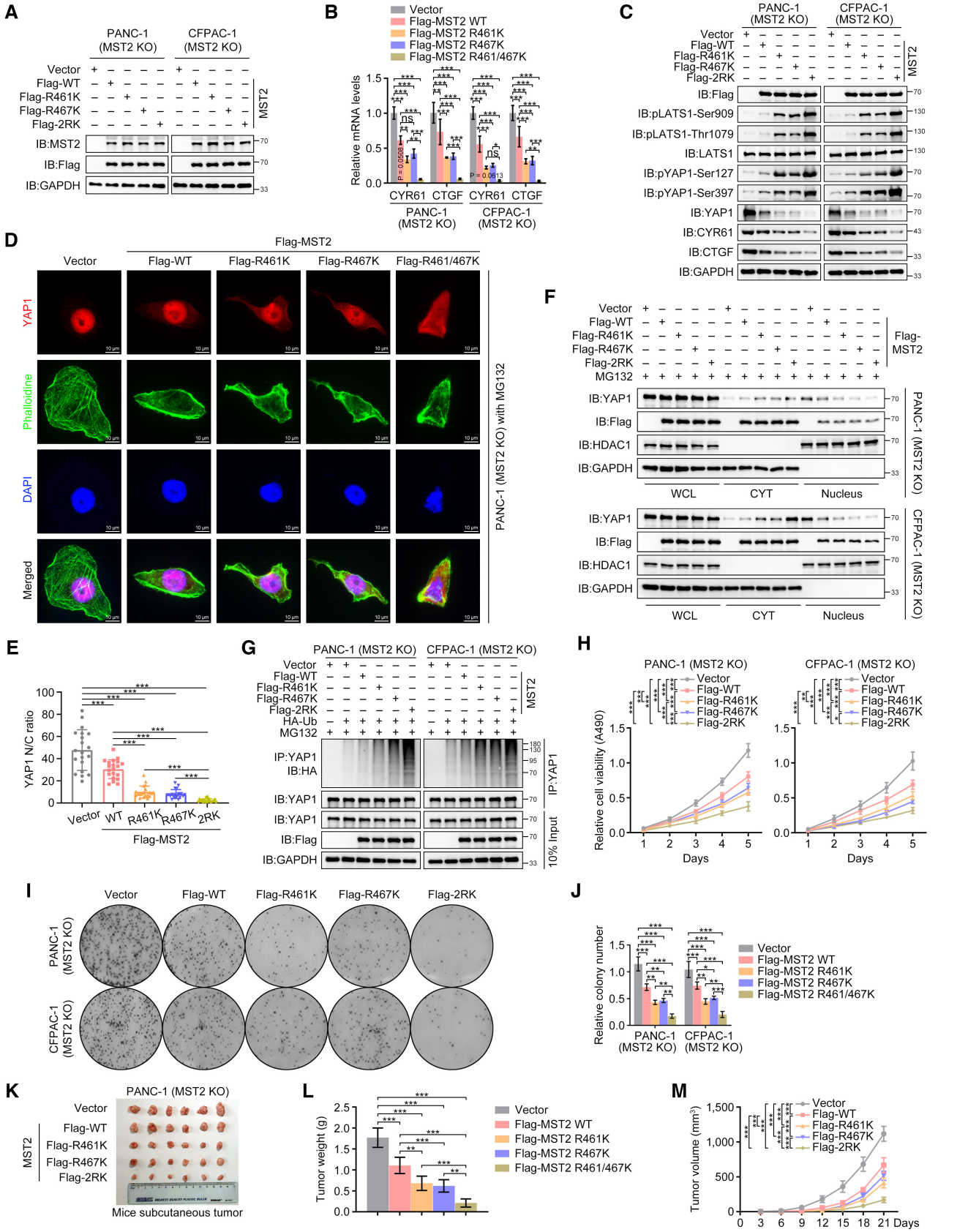
A
PANC-1 (MST2 KO)
CFPAC-1 (MST2 KO)
Vector
Flag-WT
Flag-R461K
Flag-R467K
Flag-2RK
MST2
IB:MST2
IB:Flag
IB:GAPDH
B
Vector
Flag-MST2 WT
Flag-MST2 R461K
Flag-MST2 R467K
Flag-MST2 R461/467K
Relative mRNA levels
CYR61
CTGF
PANC-1 (MST2 KO)
CFPAC-1 (MST2 KO)
C
IB:pLATS1-Ser909
IB:pLATS1-Thr1079
IB:LATS1
IB:pYAP1-Ser127
IB:pYAP1-Ser397
IB:YAP1
IB:CYR61
IB:CTGF
D
Flag-MST2
Vector
Flag-WT
Flag-R461K
Flag-R467K
Flag-R461/467K
YAP1
Phalloidine
DAPI
Merged
PANC-1 (MST2 KO) with MG132
E
YAP1 N/C ratio
Vector
WT
R461K
R467K
2RK
Flag-MST2
F
MG132
Flag-MST2
IB:HDAC1
WCL
CYT
Nucleus
PANC-1 (MST2 KO)
CFPAC-1 (MST2 KO)
G
HA-Ub
IP:YAP1
IB:HA
10% Input
H
Relative cell viability (A490)
Days
I
J
Relative colony number
K
Mice subcutaneous tumor
L
Tumor weight (g)
M
Tumor volume (mm³)
Days

Figure 4.

Figure 4. The SDMA of MST2 inhibits the activation of Hippo signaling pathway.

A The indicated plasmids were separately transfected into MST2-KO PANC-1 and CFPAC-1. After 72 h, the cells were extracted proteins to verify the transfection efficiency. Immunoblotting analysis was repeated three times independently.

B The indicated plasmids were separately transfected into MST2-KO PANC-1 and CFPAC-1. Then the cells were extracted RNA for qRT–PCR after 48 h. Data were shown as mean ± SD (n = 3 biological replicates). ns, not significant; *P < 0.05; **P < 0.01; ***P < 0.001. The statistical significance was tested by the two-way ANOVA.

C The indicated plasmids were separately transfected into MST2-KO PANC-1 and CFPAC-1. After 72 h, the cells were extracted proteins to detect the changes of Hippo signaling pathway. Immunoblotting analysis was repeated three times independently.

D–G The indicated plasmids were separately transfected into MST2-KO cells and the cells were treated with 10 μM MG132. After 72 h, the cells were transferred to the cell culture slides for immunofluorescence. The representative images (D) and the quantification (E) of 20 cells were shown in the figure. Scale bar: 10 μm. Nucleocytoplasmic separation was performed to detect YAP1 localization (F). YAP1 was purified to detect the ubiquitination level (G). Immunoblotting analysis was repeated three times independently. The statistical significance was tested by the one-way ANOVA (E). ***P < 0.001. Data were shown as mean ± SD (n = 20 biological replicates).

H–J MST2-KO cells transfected with the indicated plasmids were used for MTS (H) and colony formation assay (I and J). Data were shown as mean ± SD (n = 3 biological replicates). *P < 0.05; **P < 0.01; ***P < 0.001. The statistical significance was tested by the two-way ANOVA.

K–M MST2-KO PANC-1 cells were injected s.c. into the nude mice after infecting the indicated lentivirus. When tumors were visible, tumor volumes were measured every 3 days (M). Tumors were harvested, photographed (K), and weighed (L) at day 21. Data were shown as mean ± SD (n = 6). **P < 0.01; ***P < 0.001. The statistical significance was tested by the one-way ANOVA (L) and the two-way ANOVA (M).

Source data are available online for this figure.

PRMT5 suppresses MST2 autophosphorylation and kinase activity by blocking symmetrical di-methylated MST2 homodimerization.

PRMT5 inactivates Hippo signaling pathway via inducing MST2 SDMA

To clarify that PRMT5 regulated the Hippo signaling pathway by methylating MST2, wild-type and MST2-KO pancreatic cancer cells were treated with GSK3326595, and then the changes of the Hippo pathway were observed. The results showed that the expression of CYR61 and CTGF was only slightly reduced after GSK3326595 treatment in the MST2-KO pancreatic cancer cells (Appendix Fig S1F and G), and the level of pLATS1-Ser909, pLATS1-Thr1079, pYAP1-Ser127, pYAP1-Ser397, and YAP1 also showed a relatively small change (Appendix Fig S1G). In addition, most of YAP1 remained in the cell nucleus even though PRMT5 was inhibited in the MST2-KO cells (Appendix Fig S1H–J). We also discovered that GSK3326595 only mildly increased the ubiquitination level of YAP1 after MST2 was deleted (Appendix Fig S1K). Similarly, the consistent results were also observed *in vivo* experiments, which showed that GSK3326595 suppressed observably the growth of WT PANC-1 xenografts but had the limited effect on MST2-KO PANC-1 xenografts (Appendix Fig S1L–N). These results suggested that the effect of PRMT5 on Hippo signaling pathway was mediated by MST2, but not exclusively, and might also include other regulative manners, but all regulative manners depended on the arginine methyltransferase activity of PRMT5. Additionally, this conclusion was further confirmed on MST2 methylation-deficient background. The results showed that 2RK mutant significantly activated the Hippo pathway and inhibited the expression of its downstream genes compared to WT, while GSK3326595 not only could function to a certain extent in MST2-KO cells but also enhanced the effect of WT (Appendix Fig S1O and P). And GSK3326595 also further activated the Hippo pathway and inhibited the expression of its downstream genes on the MST2 methylation-deficient background (Appendix Fig S1O and P). Therefore, we believe that PRMT5 regulates the Hippo signaling pathway not only by catalyzing MST2 methylation but also in other ways.

PRMT5 and MST2-SDMA are elevated but pMST2-Thr180 is reduced in PDAC

Then the correlation among PRMT5, SDMA and pMST2-Thr180 was further clarified in the clinical specimens of pancreatic cancer. The tissue microarrays containing 37 pancreatic cancer patients were respectively stained by anti-PRMT5 antibody, anti-SDMA antibody and anti-pMST2-Thr180 antibody. The IHC analysis showed that the level of PRMT5 was positively correlated with SDMA but negatively correlated with pMST2-Thr180 (Fig 7A and B, Appendix Fig S2A–C). Moreover, 12 pairs of pancreatic cancer tissues and their matched para-carcinoma tissues were collected and extracted proteins for Co-IP and Western blot analysis. The results demonstrated that the level of PRMT5 and total SDMA was up-regulated in pancreatic cancer tissues (Fig 7C and D). More importantly, MST2 was symmetrically di-methylated at higher levels in pancreatic cancer tissues than that in their matched para-carcinoma tissues, whereas the phosphorylation level of MST2 at Thr180 was just opposite to its SDMA level (Fig 7C and D). These data further suggested PRMT5 catalyzed MST2 SDMA and blocked its homodimerization to suppress MST2 autophosphorylation and kinase activity, thereby inhibiting the phosphorylation cascade and inactivating the Hippo pathway.

GSK3326595 suppresses the progression of pancreatic cancer

To investigate the therapeutic effect of GSK3326595 in pancreatic cancer, the viable human-derived pancreatic cancer tissue fragments were transplanted subcutaneously into immunodeficient mice (NOG mice) to construct patient-derived tumor xenograft (PDX) model (Fig 7E). Then NOG mice were randomly divided into two groups and respectively treated with DMSO and GSK3326595. The results showed GSK3326595 significantly impeded the development and progression of pancreatic cancer (Fig 7F–H). And IHC analysis of xenografts was consistent with the above clinical specimens, which showed that GSK3326595 suppressed the level of total SDMA and increased the level of pMST2-Thr180 *in vivo* (Fig 7I and J, Appendix Fig S2D). Together, our data highlighted that MST2 SDMA mediated by PRMT5 played a crucial role in the progression of pancreatic cancer.

Discussion

The Hippo signaling axis acts as a canonical tumor suppressor pathway that modulates cell proliferation, tissue homeostasis, and organ development (Fang *et al*, 2018). However, due to a variety of complicative reasons, this tumor suppressor pathway is frequently inactivated in many types of tumors to cause tumor progression, including pancreatic cancer (Ansari *et al*, 2019). Research has

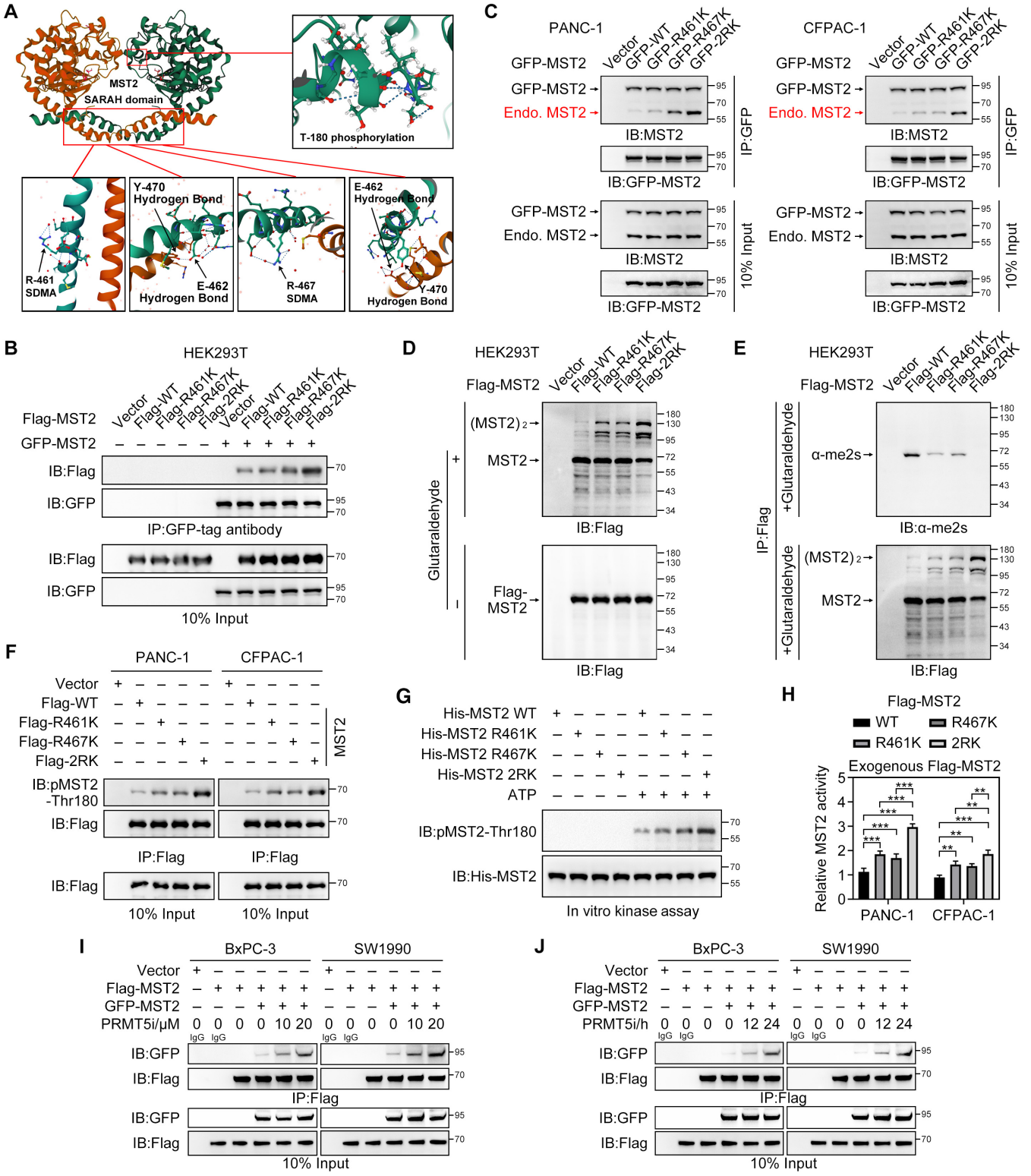

Figure 5.

Figure 5. SDMA suppresses MST2 autophosphorylation and kinase activity by decreasing the level of MST2 homodimer.

A MST2 monomers were assembled into homodimers through the SARAH domain. E-462 and Y-470 rather than R-461 and R-467 led to H-bonding between the SARAH domains in the trans configuration of MST2 homodimer. The crystal structure of MST2 protein and the details of the SARAH domain-mediated homodimer are derived from RCSB Protein Data Bank (RCSB PDB: 4LGD and 4L0N).

B HEK293T was transfected with the indicated plasmids. Then, Flag-MST2 co-precipitated by GFP-MST2 was detected. Immunoblotting analysis was repeated three times independently.

C PANC-1 and CFPAC-1 were transfected with the indicated plasmids. Then, endogenous MST2 (Endo. MST2) co-precipitated by GFP-MST2 was detected. Immunoblotting analysis was repeated three times independently.

D, E HEK293T transfected with the indicated plasmids were lysed with the mild lysis buffer. The lysates were treated with or without 0.05% glutaraldehyde for cross-linking. Then, monomer and dimer of MST2 were detected (D) and SDMA of MST2 was analyzed by native PAGE (E). Monomer and dimer of MST2 were marked by arrows. Immunoblotting analysis was repeated three times independently.

F PANC-1 and CFPAC-1 were transfected with the indicated plasmids for 72 h. Then, the phosphorylation level of Flag-MST2 at Thr180 was detected by anti-pMST2-Thr180 antibody. Immunoblotting analysis was repeated three times independently.

G Recombinant His-MST2 was expressed in *E. coli* BL21 and purified by His-tag Protein Purification Kit. Then, the purified proteins were incubated with or without ATP for kinase assay *in vitro*. Immunoblotting was repeated three times independently.

H PANC-1 and CFPAC-1 were transfected with the indicated plasmids. Flag-MST2 were purified to detect the kinase activity. Data were shown as mean ± SD ($n = 3$ biological replicates). $^{**}P < 0.01$; $^{***}P < 0.001$. The statistical significance was tested by the two-way ANOVA.

I, J BxPC-3 and SW1990 were transfected with the indicated plasmids. Then, the cells were treated with GSK3326595 in an increasing concentration gradient manner for 24 h or an increasing time gradient manner with 20 μM. Then, GFP-MST2 co-precipitated by Flag-MST2 was detected. Immunoblotting analysis was repeated three times independently.

Source data are available online for this figure.

shown that the activation of Hippo signaling pathway depends on the kinase activity of its initiator MST2 mediated by autophosphorylation at Thr180 (Deng *et al*, 2003), and the formation of MST2 homodimer was in turn required for autophosphorylation (Zheng & Pan, 2019). In this study, we found that MST2 was symmetrically di-methylated at R461 and R467 in the C-terminal SARAH domain, catalyzed by PRMT5. And the PRMT5-mediated R461 and R467 methylation of MST2 suppressed its autophosphorylation and kinase activity through blocking MST2 homodimerization, thereby inactivating the Hippo signaling pathway and promoting the proliferation of pancreatic cancer cells *in vitro*. Furthermore, PRMT5 inhibitor suppressed the progression of pancreatic cancer in mice, which was associated with the re-activated Hippo signaling pathway. These findings reveal a new mechanism of Hippo signaling pathway inactivation and provide a new idea for the clinical treatment of pancreatic cancer with PRMT5 inhibitor (Fig 8).

It is currently known that the core kinase cassette of Hippo signaling pathway is activated by various upstream regulatory branches, such as TAO1, KIBRA, WILLIN, NF2, SCRIB, RASSF, and so on (Harvey *et al*, 2013). But more and more evidences suggest that MST2 relies on the unique autophosphorylation at Thr180 for kinase activity (Deng *et al*, 2003; Cairns *et al*, 2020; Tran *et al*, 2020), which demonstrates that self-control of the Hippo signaling pathway may be more meaningful than the influence of the external factors. MST2 was also indeed autophosphorylated at Thr180 in pancreatic cancer cells in our study. In addition, series of studies reveal that SARAH domain of MST2 mediates its homodimerization and thereby inducing autophosphorylation (Creasy *et al*, 1996; Praskova *et al*, 2004; Ni *et al*, 2013; Bae & Luo, 2018; Zheng & Pan, 2019). But our study discovered that MST2 could be methylated at R461 and R467, located exactly within the SARAH domain, which blocked the formation of MST2 homodimer and consequently suppressed MST2 autophosphorylation at Thr180. Interestingly, a previous report showed that MST2 autophosphorylation could be triggered so long as the kinase domains of MST1/2 were close sufficiently to achieve the effective local concentration, rather than a specific protein assembly (Tran *et al*, 2020), which suggested that SARAH domain was not essential for MST2 autophosphorylation. But it is generally accepted that MST2 only relies on the SARAH domain for the increasing kinase domain proximity in the cell. In agreement with the report, our research indicated that SDMA blocked MST2 homodimerization to cause the farther kinase domain proximity and the little autophosphorylation. Besides, SARAH domain of MST2 is considered as a universal binding partner that also forms heterodimers with other SARAH domain-bearing proteins, for example MST1 (Rawat *et al*, 2016), RASSF (Sánchez-Sanz *et al*, 2016), and SAV1 (Bae *et al*, 2017). Here we only discussed in depth the effect of MST2 methylation on its homodimerization, because we held the opinion that the methylation of both monomers had a greater resistance for dimerization than the methylation of only one monomer.

Post-translational modifications (PTMs), the core of many cellular signaling events, involve multifarious modes such as phosphorylation, ubiquitination, acetylation, methylation, and glycosylation, which frequently serves as a key mechanism to adjust cell life activities (Vu *et al*, 2018). Protein arginine methylation, as a PTM, catalyzed by the PRMT family, exists ubiquitously in the nucleus and cytoplasm. As the major type II PRMT that catalyzes symmetric dimethylarginine, PRMT5 regulates various primary cellular processes including DNA damage and repair, RNA processing, and protein stability (Yin *et al*, 2021). And PRMT5 dysregulation is closely related to the occurrence and development of tumors (Liu *et al*, 2016). In our study, we discovered that the symmetrically di-methylated MST2 catalyzed by PRMT5 lost the autophosphorylated ability and kinase activity, which resulted in the inactivation of the Hippo signaling pathway from the source and thereby promoting the progression of pancreatic cancer. Notably, this study is not the first to report that components of the Hippo signaling pathway are modified after protein translation. Jin *et al* showed that oxidative stress-CBP signal axis induces MOB1 acetylation to promote the activation of the Hippo signaling pathway (Jin *et al*, 2022). Fang *et al* found that SET1A promotes YAP1 mono-methylation at K342 to modulate its activation and leads to tumorigenesis (Fang *et al*, 2018). And YAP1 can also be acetylated and deacetylated at lysine 494 and 497 by

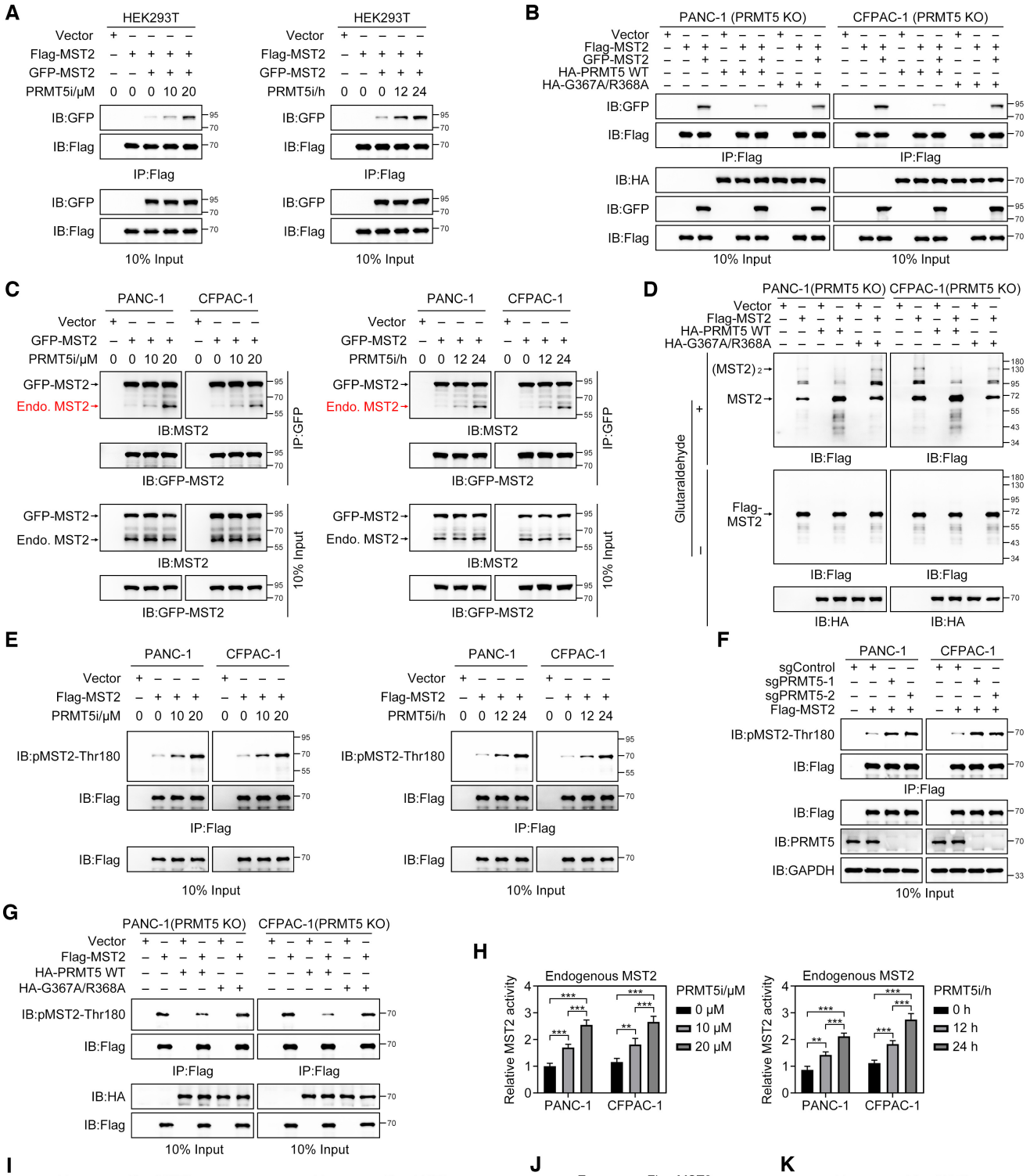
A
HEK293T
Vector
Flag-MST2
GFP-MST2
PRMT5i/μM 0 0 0 10 20
PRMT5i/h 0 0 0 12 24
IB:GFP
IB:Flag
IP:Flag
10% Input
B
PANC-1 (PRMT5 KO)
CFPAC-1 (PRMT5 KO)
HA-PRMT5 WT
HA-G367A/R368A
IB:HA
C
PANC-1
CFPAC-1
GFP-MST2→
Endo. MST2→
IB:MST2
IB:GFP-MST2
IP:GFP
10% Input
D
(MST2)2→
MST2→
Flag-MST2→
Glutaraldehyde
E
IB:pMST2-Thr180
F
sgControl
sgPRMT5-1
sgPRMT5-2
IB:PRMT5
IB:GAPDH
G
H
Endogenous MST2
Relative MST2 activity
PRMT5i/μM
0 μM
10 μM
20 μM
PRMT5i/h
0 h
12 h
24 h
I
Exogenous Flag-MST2
J
sgControl
sgPRMT5-1
sgPRMT5-2
K
EV
PRMT5 WT
G367A/R368A
ns

Figure 6.

Figure 6. PRMT5 suppresses MST2 autophosphorylation and kinase activity by blocking symmetrical di-methylated MST2 homodimerization.

A HEK293T cells were transfected with the indicated plasmids. Then, the cells were treated with GSK3326595 in an increasing dosage manner for 24 h or an increasing time manner with 20 μM. Then, GFP-MST2 co-precipitated by Flag-MST2 was detected. Immunoblotting analysis was repeated three times independently.

B PRMT5-KO cells were transfected with the indicated plasmids. Then, GFP-MST2 co-precipitated by Flag-MST2 was detected by Co-IP and immunoblotting analysis. Immunoblotting analysis was repeated three times independently.

C PANC-1 and CFPAC-1 transfected with the indicated plasmids were treated with GSK3326595 in an increasing dosage manner for 24 h or an increasing time manner with 20 μM. Then, endogenous MST2 (Endo. MST2) co-precipitated by GFP-MST2 was detected. Immunoblotting analysis was repeated three times independently.

D PRMT5-KO cells were transfected with the indicated plasmids. Then the cells were lysed with the mild lysis buffer. The lysates were treated with or without 0.05% glutaraldehyde for cross-linking. Then, monomer and dimer of MST2 were detected by native PAGE. Monomer and dimer of MST2 were marked by arrows. Immunoblotting analysis was repeated three times independently.

E PANC-1 and CFPAC-1 expressed Flag-MST2 were treated with GSK3326595 in the increasing dosage manner for 24 h or the increasing time manner with 20 μM. Then, the phosphorylation level of Flag-MST2 at Thr180 was detected. Immunoblotting analysis was repeated three times independently.

F PRMT5-KO cells expressed Flag-MST2 were detected the phosphorylation level of Flag-MST2 at Thr180. Immunoblotting was repeated three times independently.

G PRMT5-KO cells were transfected with the indicated plasmids. Then, the phosphorylation level of Flag-MST2 at Thr180 was detected. Immunoblotting analysis was repeated three times independently.

H PANC-1 and CFPAC-1 were treated with GSK3326595 in the increasing dosage manner for 24 h or the increasing time manner with 20 μM. Then, endogenous MST2 was purified to detect its kinase activity. Data were shown as mean ± SD (n = 3 biological replicates). $^{**}P < 0.01$; $^{***}P < 0.001$. The statistical significance was tested by the two-way ANOVA.

I PANC-1 and CFPAC-1 expressed Flag-MST2 were treated with GSK3326595 in the increasing dosage manner for 24 h or the increasing time manner with 20 μM. Then, Flag-MST2 was purified to detect its kinase activity. Data were shown as mean ± SD (n = 3 biological replicates). $^{*}P < 0.05$; $^{**}P < 0.01$; $^{***}P < 0.001$. The statistical significance was tested by the two-way ANOVA.

J, K The kinase activity of Flag-MST2 was detected after PRMT5 was knocked out (J) or PRMT5 WT/mutant was overexpressed (K). Data were shown as mean ± SD (n = 3 biological replicates). ns, not significant; $^{**}P < 0.01$; $^{***}P < 0.001$. The statistical significance was tested by the two-way ANOVA.

Source data are available online for this figure.

CBP/p300 and SIRT1, respectively (Hata *et al*, 2012). While our study reveals a novel mechanism of the Hippo signaling pathway inactivation at the source, which provides a new idea for re-activating the dysregulated Hippo signaling pathway and inhibiting pancreatic cancer progression.

Pancreatic cancer is a highly malignant tumor that is insensitive to existing treatment methods, including chemoradiotherapy, targeted therapy, and immunotherapy (Neoptolemos *et al*, 2018). Therefore, it is urgent to explore a new treatment method to improve the prognosis of pancreatic cancer. One previous report showed that the aberrant PRMT5 expression caused the worse survival and targeting PRMT5 prevented cancer growth across multiple cancers (Lee *et al*, 2021). Here our study showed that the expression level of PRMT5 was elevated in pancreatic cancer tissues compared to para-carcinoma tissues, so PRMT5 might be a potential target for pancreatic cancer. Importantly, targeting PRMT5 inhibits pancreatic cancer progression through multiple complex mechanisms, for example regulating alternative RNA splicing (Fedoriw *et al*, 2019), improving gemcitabine sensitivity (Wei *et al*, 2020), reversing epithelial-mesenchymal transition (Ge *et al*, 2020), but these results are limited to preclinical studies resulting in the lack of clinical data. Recently, phase I trials of PRMT5 inhibitors (GSK3326595 and JNJ64619178) have been reported in head and neck squamous cell carcinoma, breast and adenoid cystadenocarcinoma to explore their activity and safety (Siu *et al*, 2019; Villar *et al*, 2020), and the similar clinical trials with PF-06939999 (NCT03854227), PRT811 (NCT04089449) and PRT543 (NCT03886831) are also currently ongoing (Lee *et al*, 2021). Similarly, we want to advance the translation of PRMT5 inhibitors from basic researches to clinical trials in pancreatic cancer, which requires the better mechanism elucidation of PRMT5 promoting pancreatic cancer progression. Our study showed that specific PRMT5 inhibitor GSK3326595 re-activated the

Figure 7. PRMT5 and MST2-SDMA are elevated but pMST2-Thr180 is reduced in PDAC, and GSK3326595 suppresses the progression of pancreatic cancer.

A, B The representative IHC images of PRMT5, α-me2s and pMST2-Thr180 proteins on TMA (n = 37) of pancreatic cancer specimens were shown (A). Scale bars were indicated in the figure. The heatmap showed IHC score of PRMT5, α-me2s and pMST2-Thr180 proteins on TMA (n = 37) of pancreatic cancer specimens (B).

C Twelve pairs of pancreatic cancer tissues and their matched para-carcinoma tissues were extracted proteins. MST2 was immunopurified to compare the level of α-me2s and phospho-Thr180 between cancer tissues and para-carcinoma tissues. Relative ratio was quantified and normalized to MST2. The level of PRMT5 and total α-me2s was also compared. Immunoblotting was repeated technically three times independently. N = 12 biological replicates.

D Relative α-me2s level of MST2, relative pMST2-Thr180 level of MST2, relative PRMT5 level, and relative total α-me2s level of pancreatic cancer tissues and para-carcinoma tissues were quantified and shown as the violin plots. The statistical significance was tested by the paired t-test. Immunoblotting was repeated technically three times independently. N = 12 biological replicates. $^{**}P < 0.01$; $^{***}P < 0.001$.

E The schematic showed the basic procedure of constructing patient-derived tumor xenograft (PDX) model.

F–H PDX mice were randomized in the following two groups after xenografts grew to a size of 50 mm^3, with six mice in each group: (1) DMSO; (2) GSK3326595 100 mg/kg every 3 days intravenous injection. The size of xenografts was measured and summarized every 3 days (G). After 30 days, all mice were euthanatized for photographing and the xenografts were also harvested for photographing (F) and weighing (H). Data were shown as mean ± SD (n = 6). $^{***}P < 0.001$. The statistical significance was tested by the unpaired t-test (H) and the two-way ANOVA (G). Arrows indicated the xenografts subcutaneously in mice.

I The representative IHC images of total α-me2s (CST) and pMST2-Thr180 on the xenografts of PDX mice (n = 6) were shown (Mouse No. 1). Scale bars were indicated in the figure.

J IHC score of total α-me2s (CST) and pMST2-Thr180 on the xenografts of PDX mice (n = 6) were summarized and analyzed. Data were shown as mean ± SD (n = 6). $^{***}P < 0.001$. The statistical significance was tested by the two-way ANOVA.

Source data are available online for this figure.

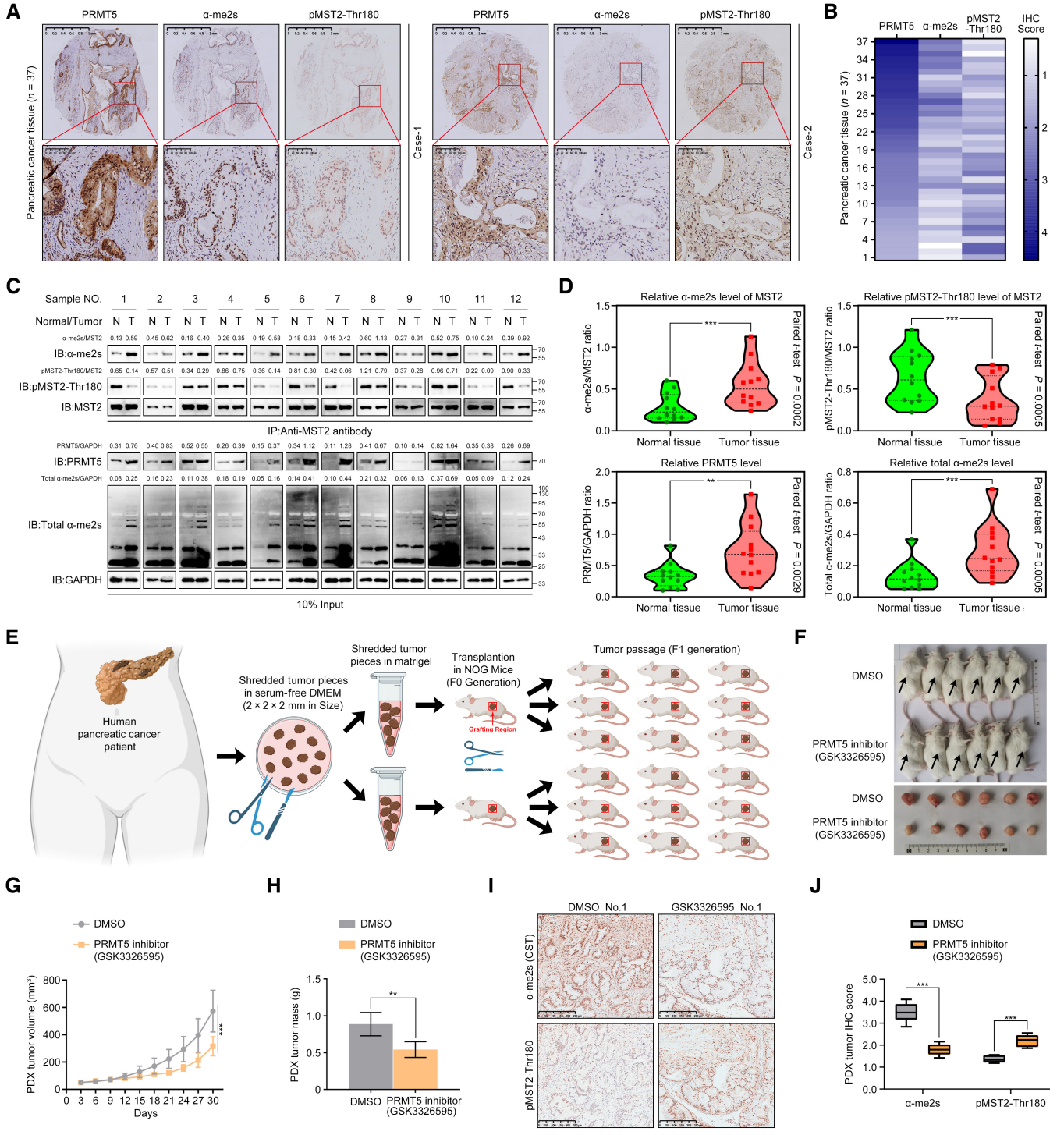

Figure 7.

dysregulated Hippo signaling pathway and suppressed the growth of human-derived pancreatic cancer xenografts in immunodeficient mice, which further laid the theoretical foundation for the clinical application of PRMT5 inhibitors in pancreatic cancer.

Although the study reveals that the symmetric di-methylarginine catalyzed by PRMT5 blocks MST2 homodimerization, leading to the decreased autophosphorylation and kinase activity, there are still several limitations in this work. Firstly, protein arginine methylation is divided into three types, including MMA, ADMA and SDMA. Here we only examined the effect of SDMA on MST2, but it was unknown as regard whether MST2 could be mono-methylated or asymmetrically di-methylated. Secondly, currently available

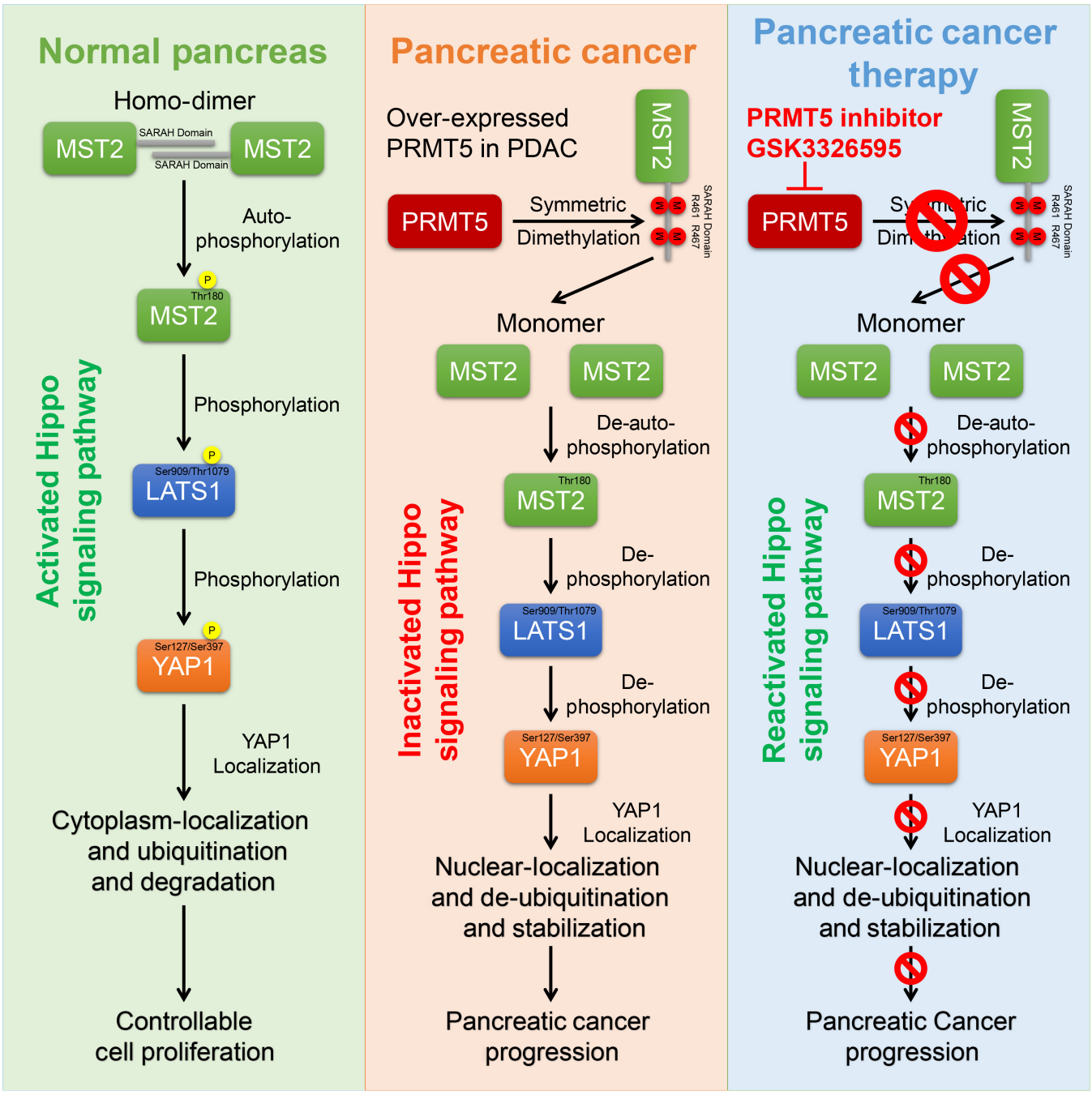

Figure 8. Regulation and control mechanism illustrating how PRMT5 inactivates the Hippo signaling pathway and promotes pancreatic cancer progression. In normal pancreas, MST2 is autophosphorylated and activated after homodimerization through SARAH domain and then induces the phosphorylation of downstream LATS1 and YAP1 step by step, which causes YAP1 to be localized in the cytoplasm for ubiquitinated degradation and controls cell proliferation. However, overexpressed PRMT5 in pancreatic cancer catalyzes MST2 symmetric dimethylation in its SARAH domain, which inactivates Hippo signaling pathway by preventing MST2 homodimerization and promotes pancreatic cancer progression. PRMT5 inhibitor GSK3326595 reactivates Hippo signaling pathway and inhibits pancreatic cancer progression by preventing MST2 methylation.

anti-pMST2-Thr180 antibodies on the market lack specificity, which can recognize both pMST2-Thr180 and pMST1-Thr183. In this study, endogenous and exogenous MST2 could be purified by Co-IP to eliminate MST1 interference, but IHC staining of pancreatic cancer tissues failed to remove MST1 background. Thirdly, the whole proteome analyses show the reversibility of arginine methylation, whereas proteins that mediate arginine demethylation have not been well characterized. We were also

unable to pinpoint which proteins induce arginine demethylation in MST2.

Materials and Methods

Cell lines and cell culture

Human cell lines HEK293T (Cat# CL-0005) (RRID:CVCL_0063), PANC-1 (Cat# CL-0184) (RRID:CVCL_0480), CFPAC-1 (Cat# CL-0059) (RRID:CVCL_1119), BxPC-3 (Cat# CL-0042) (RRID:CVCL_0186), and SW1990 (Cat# CL-0448B) (RRID:CVCL_1723) were purchased from Procell Life Science&Technology Co., Ltd (Wuhan, China). All cell lines were cultured in complete Dulbecco's modified Eagle medium (DMEM, Gibco, USA) containing 10% fetal calf serum (FBS, Gibco, USA), 1% Penicillin–Streptomycin (Thermo Fisher Scientific, USA) and 5 μg/ml plasmocin (InvivoGen, France). Trypsin Solution (Gibco, USA) was used for cell dissociation and routine cell culture passaging. Cells were cultured in the 37°C and 5% CO_2 incubator. All cell lines have been authenticated by STR profiling and excluded from mycoplasma contamination.

Clinical specimen collection

The informed consent was obtained from all subjects. The ethics of using human tissues was authorized by the local ethics committee (Tongji Medical College, Huazhong University of Science and Technology, China) (reference number: UHCT-IEC-SOP-016-03-01). Pancreatic cancer tissues and para-carcinoma tissues were from Department of Pancreatic Surgery, Union Hospital, Tongji Medical College, Huazhong University of Science and Technology. Twelve pairs of pancreatic ductal adenocarcinoma (PDAC) tissues and their matched para-carcinoma tissues were collected for the construction of patient-derived tumor xenograft (PDX) model. And the tissues were extracted proteins for Co-IP and Western blot analysis.

Antibodies and chemicals

The used antibodies in this study were shown below: α-me2s (Cell Signaling Technology Cat# 13222, RRID:AB_2714013; 1:1,000 dilution for WB, 1:500 dilution for IHC), α-me2s (Antibodies, ABIN870728; 1:1,000 dilution for WB, 1:100 dilution for IHC), MST2 (Proteintech Cat# 12097-1-AP, RRID:AB_2198801; 1:1,000 dilution for WB), MST2 (ABclonal Cat# A9036, RRID:AB_2863645; 1:2,000 dilution for WB), MST2 (Cell Signaling Technology Cat# 3952, RRID:AB_2196471; 1:25 dilution for IP), Flag (Proteintech Cat# 20543-1-AP, RRID:AB_11232216; 1:2,000 dilution for WB), GAPDH (Proteintech Cat# 10494-1-AP, RRID:AB_2263076; 1:20,000 dilution for WB), pLATS1-Ser909 (Signalway Antibody, C13033; 1:500 dilution for WB), pLATS1-Thr1079 (Signalway Antibody, C13032; 1:500 dilution for WB), LATS1 (Proteintech Cat# 17049-1-AP, RRID:AB_2281011; 1:1,000 dilution for WB), pYAP1-Ser127 (Signalway Antibody, 11952; 1:1,000 dilution for WB), pYAP1-Ser397 (Signalway Antibody, 13443; 1:1,000 dilution for WB), YAP1 (Proteintech Cat# 13584-1-AP, RRID:AB_2218915; 1:5,000 dilution for WB, 1:25 dilution for IP), CYR61 (Proteintech Cat# 26689-1-AP, RRID:AB_2880604; 1:2,000 dilution for WB), CTGF (Proteintech Cat# 25474-1-AP, RRID:AB_2918089; 1:2,000 dilution for WB), HDAC1 (Proteintech Cat# 10197-1-AP, RRID:AB_2118062; 1:10,000 dilution for WB), HA (Proteintech Cat# 51064-2-AP, RRID:AB_11042321; 1:2,000 dilution for WB), GFP (Proteintech Cat# 50430-2-AP, RRID:AB_11042881; 1:2,000 dilution for WB, 1:25 dilution for IP), pMST2-Thr180 (Affinity Biosciences Cat# AF2367, RRID:AB_2845381; 1:500 dilution for WB, 1:100 dilution for IHC), His (Proteintech Cat# 66005-1-Ig, RRID:AB_11232599; 1:5,000 dilution for WB), PRMT5 (Proteintech Cat# 18436-1-AP, RRID:AB_2171798; 1:3,000 dilution for WB, 1:500 dilution for IHC), PRMT7 (Proteintech Cat# 67669-1-Ig, RRID:AB_2882865; 1:1,000 dilution for WB), PRMT9 (ABclonal Cat# A10491, RRID:AB_2758040; 1:1,000 dilution for WB), MEP50 (Proteintech Cat# 10115-1-AP, RRID:AB_2215725; 1:500 dilution for WB), Myc (Proteintech Cat# 16286-1-AP, RRID:AB_11182162; 1:2,000 dilution for WB), GST (Proteintech Cat# 10000-0-AP, RRID:AB_11042316; 1:2,000 dilution for WB), MST1 (ABclonal Cat# A8043, RRID:AB_2772441; 1:2,000 dilution for WB), SAV1 (ABclonal Cat# A9980, RRID:AB_2772146; 1:2,000 dilution for WB), AURKB (Abcam, ab287960; 1:1,000 dilution for WB), ANKRD1 (Proteintech Cat# 11427-1-AP, RRID:AB_2227402; 1:2,000 dilution for WB), AffiniPure Goat Anti-Rabbit IgG (H+L) (AMSBIO Cat# BA1039, RRID:AB_10890454; 1:5,000 dilution for WB), AffiniPure Goat Anti-Mouse IgG (H+L) (AMSBIO Cat# BA1038, RRID:AB_10891748; 1:5,000 dilution for WB), CY3 Conjugated AffiniPure Goat Anti-rabbit IgG (H+L) (AMSBIO Cat# BA1032, RRID:AB_10890054; 1:500 dilution for IF), Mouse Anti-rabbit IgG (Conformation Specific) (L27A9) mAb (HRP Conjugate) (Cell Signaling Technology Cat# 5127, RRID:AB_10892860; 1:2,000 dilution for WB after IP). The used chemicals in this study were shown below: Adenosine-Dialdehyde (AdOx, Selleck, S8608), MG132 (Med Chem Express, HY-13259), GSK3326595 (Pemrametostat, EPZ015938, Selleck, S8664).

CRISPR/Cas9 technique

Single guide RNAs (sgRNAs) of Control (sgControl), MST2 (sgMST2-1 and sgMST2-2), PRMT5 (sgPRMT5-1 and sgPRMT5-2), PRMT7 (sgPRMT7-1 and sgPRMT7-2) and PRMT9 (sgPRMT9-1 and sgPRMT9-2) were designed and purchased from Merck (https://www.sigmaaldrich.cn/CN/zh). Then sgRNAs were cloned into lenti-CRISPR v2 vector (#52961, Addgene, USA). The sequences of sgRNAs are shown in Table 1.

Plasmid transfection

Plasmids expressed exogenous proteins were ordered from Shanghai Gene Chem Co., Ltd and Bio-Transduction Lab, Wuhan Institute of Biotechnology, Hubei Wuhan. The indicated plasmids were transfected into pancreatic cancer cells or HEK293T cells after incubating for 20 min with Lipofectamine 2000 (Thermo Fisher Scientific, USA). After 6 h of transfection, the transfected medium was replaced with DMEM containing 10% FBS. Then the cells were treated with puromycin (Solarbio, China) at a working concentration of 3 μg/ml to eliminate non-transfected cells.

Lentiviral infection

Pancreatic cancer cells were cultured in 6-well plates. The next day, the appropriate amounts of lentiviral particles was used to infect

Table 1. The sequences of sgRNAs, related to CRISPR/Cas9 technique of STAR Methods section.

sgRNA (human)	The sequences of sgRNA (5′-3′)
sgControl	CGCTTCCGCGGCCCGTTCAA
sgMST2-1	GAGGAACAGCAACGAGAAT
sgMST2-2	AATCATCGGACCAAAGTTC
sgPRMT5-1	AGCATACAGCTTTATCCGC
sgPRMT5-2	CCCTTGGCAAAGAGTTCAT
sgPRMT7-1	AGCTCTCCACGTCAACGGG
sgPRMT7-2	AGGTTCAAACCGCCTGCTA
sgPRMT9-1	ACGTGTTAGATGTGTCCGA
sgPRMT9-2	GACCAGCATCGTATTGCTC

pancreatic cancer cells after the addition of the infection medium composed of complete DMEM and HiTrans G reagent (25:1 ratio). After 72 h, puromycin (10 μg/ml) or ampicillin (10 μg/ml) was used to select infected successfully pancreatic cancer cells.

Western blot analysis

Pancreatic cancer cells were harvested and lysed in an ice bath for 30 min with RIPA Lysis Buffer (Beyotime, China) containing 50 mM Tris (pH 7.4), 150 mM NaCl, 1% Triton X-100, 1% sodium deoxycholate, 0.1% SDS, sodium orthovanadate, sodium fluoride, EDTA, leupeptin and 1% protease inhibitor cocktails. The cell lysate was recycled back into centrifuge tubes for further ultrasonication. Then cell lysate was centrifuged for 10 min at 16,000 *g* at 4°C and the liquid supernatant was transferred to a new centrifuge tube. The protein concentration of supernatant was quantified by BCA protein quantification assay (Beyotime, China). The remaining supernatant was added into a quarter volume of 5× Protein Loading Buffer (Beyotime, China) and boiled for 10 min at 95°C. Then sodium dodecyl sulfate polyacrylamide gel electrophoresis (SDS–PAGE) was performed to separate the protein samples according to different molecular weights. The separated protein in gel was transferred onto PVDF membranes (Beyotime, China). The PVDF membranes were blocked for 1 h at room temperature with 5% skim milk powder. Then the PVDF membranes were incubated with primary antibodies at 4°C overnight after washing the milk with TBST buffer. The next day, the PVDF membranes were washed three times with TBST buffer and incubated with horseradish peroxidase-conjugated secondary antibodies for 1 h at room temperature. After washing again with TBST buffer, the protein bands were added dropwise ECL reagent (Thermo Fisher Scientific, USA) and visualized by Bio-Rad Image Lab.

Native PAGE

Flag-MST2 plasmids were transfected into pancreatic cancer cells or HEK293T cells. After 3 days, cells were lysed in an ice bath for 30 min with Cell Lysis Buffer for Western and IP without Inhibitors (P0013J, Beyotime, China). The lysates were incubated for 10 min with 0.05% glutaraldehyde (Sigma-Aldrich, USA) at room temperature for cross-linking. Then the lysates were added into a quarter volume of 5× Non-denatured Gel Sample Loading Buffer (P0016, Beyotime, China) and separated on BeyoGel™ Plus Precast PAGE Gel for Tris-Gly System (P0456S, Beyotime, China). The subsequent steps were the same as Western blot analysis.

Co-immunoprecipitation (Co-IP)

Pancreatic cancer cells were lysed by Cell Lysis Buffer for Western and IP (Beyotime, China) at 4°C for 30 min. The lysate was centrifuged for 15 min at 4°C and 12,000 rpm to discard cell-debris pellet and collect liquid supernatant. The liquid supernatant was transferred to a new centrifuge tube and incubated with primary antibodies and protein A/G agarose beads (Thermo Fisher Scientific, USA) on the rotary mixer at 4°C. After incubation for 12 h, the beads were collected by centrifugation and washed for six times with PBS buffer. Then the beads were resuspended with 1× SDS–PAGE loading buffer and boiled for 10 min at 95°C to perform Western blot analysis. BeyoMag™ Anti-Flag Magnetic Beads (P2115, Beyotime, China), BeyoMag™ Anti-HA Magnetic Beads (P2121, Beyotime, China) and BeyoMag™ Anti-Myc Magnetic Beads (P2118, Beyotime, China) were used respectively to precipitate exogenous Flag/HA/Myc-tag proteins. The magnetic beads were washed with the magnetic separator. The analysis of tryptic peptides by mass spectrometry (MS) was performed by SpecAlly Life Technology Co., Ltd, Wuhan, China. The SDMA-shotgun mass spectra are provided in Dataset EV1.

Quantitative real-time PCR (qRT–PCR)

TRIzol reagent (Thermo Fisher Scientific, USA) was used to lyse pancreatic cancer cells for extracting total RNA. The NanoDrop™ 2000/2000C Spectrophotometer (Thermo Fisher Scientific, USA) was used to determinate total RNA concentration and quality. Then, total RNA was reverse-transcribed with 5× HiScript III qRT SuperMix[a] (Vazyme, China), and PCR was performed using 2× AceQ qPCR SYBR Green Master Mix[a] (Vazyme, China). Relative gene expression levels were calculated through the $2^{-\Delta Ct}$ method after normalizing to GAPDH levels. The primer sequences for qRT–PCR are provided in Table 2.

Immunofluorescence assay

Pancreatic cancer cells were cultured sparsely and dispersedly on cell culture slides. After adhering to the slides, the cells were fixed for 30 min with 4% paraformaldehyde and permeabilized for 10 min with 0.2% Triton X-100 (Beyotime, China). Then, the cells were incubated with anti-YAP1 antibody (working concentration

Table 2. The sequences of qRT–PCR primers, related to Quantitative real-time PCR (qRT–PCR) of STAR Methods section.

Gene	Forward primer (5′-3′)	Reverse primer (5′-3′)
CYR61	ACCGCTCTGAAGGGGATCT	ACTGATGTTTACAGTTGGGCTG
CTGF	ACCGACTGGAAGACACGTTTG	CCAGGTCAGCTTCGCAAGG
AURKB	CGCAGAGAGATCGAAATCCAG	AGATCCTCCTCCGGTCATAAAA
ANRKD1	GCCTACGTTTCTGAAGGCTG	GTGGATTCAAGCATATCACGGAA
GAPDH	GGAGCGAGATCCCTCCAAAAT	GGCTGTTGTCATACTTCTCATGG

1:100) at 4°C overnight after blocking for 1 h with Goat Serum (Beyotime, China). The next day, the cells were washed for three times with PBS buffer and incubated with fluorescent secondary antibodies for 1 h at room temperature in the dark conditions. Cytoskeleton and cell nuclei were also stained with FITC-PHalloidine (Solarbio, China) and DAPI (Beyotime, China), respectively. Then cell culture slides were observed under a confocal microscopy (Andor, Dragonfly).

Subcellular fractionation

Nuclear proteins and cytoplasmic proteins were separated by Nuclear and Cytoplasmic Protein Extraction Kit (Beyotime, China). Briefly, 200 μl of reagent A containing 1% PMSF was added into 20 μl of cell pellets to lyse for 15 min on ice. Then 10 μl of reagent B was added into the lysates for 1 min on ice. The lysates were centrifuged for 5 min at 16,000 *g* at 4°C, and the supernatant was the extracted cytoplasmic proteins. After the supernatant was absorbed completely, 50 μl of nucleoprotein extraction reagent was added into the precipitation for 30 min on ice. The mixture was centrifuged for 10 min at 16,000 *g* at 4°C, and the supernatant was the extracted nuclear proteins.

MTS assay

Cell proliferation capacity was assessed through MTS assay. A count of 2,000 pancreatic cancer cells were resuspended in 100 μl of medium and cultured in 96-well plates. Then MTS reagent (Solarbio, China) was added into the 96-well plates (20 μl of MTS reagent in each well). After incubation for 4 h at 37°C, dimethylsulfoxide (Solarbio, China) was added into the 96-well plates (200 μl of dimethylsulfoxide in each well) and the plates were shaken for 30 min on the shaker in the dark conditions. Finally, the absorbency at 490 nm was measured in a microplate reader.

Colony formation assay

A count of 500 pancreatic cancer cells were cultured in 6-well plates and the medium was replaced every 3 days. After 2 weeks, the medium was removed and 4% paraformaldehyde (Beyotime, China) was added into the 6-well plates to fix pancreatic cancer cells. Then pancreatic cancer cells were stained for 30 min with Crystal Violet Staining Solution (Beyotime, China) after fixing for 30 min.

MST2 kinase activity assay

MST2 kinase activity assay was determined by Kinase-Lumi™ Max Luminescent Kinase Assay Kit (S0158S, Beyotime, China). Firstly, ATP solution was diluted to concentrations of 0, 1, 2, 4, 8, 16, 32, 64, 128, 200 μM with kinase buffer (50 mM Tris–HCl [pH 7.5], 100 mM KCl, 50 mM $MgCl_2$, 50 mM $MnCl_2$, 1 mM Na_3VO_4, 1 mM DTT, 5% glycerol). Then ATP standard curve in 100 μl reaction system containing 50 μl ATP-kinase buffer and 50 μl reaction reagent was calculated and drawn. Secondly, Flag-tagged MST2 plasmids (WT or mutant) were transfected into pancreatic cancer cells or HEK293T cells. Flag-tagged MST2 proteins (kinase) were immunoprecipitated with BeyoMag™ Anti-Flag Magnetic Beads (P2115, Beyotime, China) and eluted by 3× Flag Peptide (P9801, Beyotime, China). Similarly, Flag-tagged LATS1 proteins (substrate) were also purified and eluted as mentioned above. Then kinase, ATP, substrate and kinase buffer were mixed with a total volume of 50 μl, and 50 μl of reaction reagent was added into the mixture to incubate for 10 min at 25°C. Finally, chemiluminescent was detected by a microplate reader. The enzymatic activity was calculated on the basis of ATP consumption. The amount of enzyme required to consume 1 μmol of ATP per minute was defined as an enzyme active unit (U).

Glutathione S-transferase (GST) pull-down

Recombinant GST-MST2 proteins were expressed in *E. coli* BL21 (Cat# D0337, Beyotime) and GST-tagged proteins were purified by BeyoMag™ Anti-GST Magnetic Beads (P2138, Beyotime, China). HA-PRMT5 plasmids were transfected into HEK293T cells and HA-tagged proteins were purified by BeyoMag™ Anti-HA Magnetic Beads (P2121, Beyotime, China). Then the purified GST-MST2 proteins were incubated with the purified HA-PRMT5 proteins for 12 h on the rotary mixer at 4°C. The anti-GST magnetic beads were collected and washed for six times with PBS buffer on the magnetic separator. Next, the anti-GST magnetic beads were resuspended with 1× SDS–PAGE loading buffer and boiled for 10 min at 95°C to perform Western blot analysis and Coomassie brilliant blue staining.

Immunohistochemistry (IHC)

Pancreatic cancer tissue microarray (TMA) slides (HPanA060CS02) including 37 cases of pancreatic cancer were purchased from Shanghai Outdo Biotech Co., Ltd. Then the TMA slides and PDX mice xenografts were performed IHC staining with PRMT5, α-me2s and pMST2-Thr180 antibodies. The evaluation criterion of IHC staining intensity was based on the staining magnitude (no staining/little staining/weak staining/medium staining/strong staining) and magnification (40×/100×). IHC staining intensity was scored as follows: 0 = no staining at 40× and 100× magnification; 1 = little staining at 100× magnification; 2 = weak staining at 100× magnification; 3 = medium staining at 100× magnification; 4 = medium staining at 40× magnification; 5 = strong staining at 40× magnification. The final IHC staining index was calculated using the formula: IHC staining intensity × positive cells ratio.

In vitro kinase assay

Recombinant His-MST2 WT and its mutant proteins were expressed in *E. coli* BL21 and His-tagged proteins were purified by His-tag Protein Purification Kit (P2226, Beyotime, China). Then the purified His-MST2 WT or mutant was incubated for 1 h at 25°C in kinase buffer (50 mM Tris–HCl [pH 7.5], 100 mM KCl, 50 mM $MgCl_2$, 50 mM $MnCl_2$, 1 mM Na_3VO_4, 1 mM DTT, 5% glycerol) in the presence of 0.5 mM ATP (Solarbio, China). The reaction was stopped after adding 5× SDS–PAGE loading buffer and the samples were resolved by SDS–PAGE. The subsequent steps were the same as Western blot analysis.

In vitro methylation assay

Recombinant His-MST2 WT and its mutant proteins were expressed in *E. coli* BL21 and His-tagged proteins were purified by His-tag

Protein Purification Kit (P2226, Beyotime, China). Recombinant GST-PRMT5 (WT or the enzymatically dead mutant) and GST-MEP50 were transfected into HEK293T cells and GST-tagged proteins were purified by BeyoMag™ Anti-GST Magnetic Beads (P2138, Beyotime, China). The purified His-MST2 proteins were incubated with the purified GST-PRMT5/GST-MEP50 or GST-G367A/R368A/GST-MEP50 in the presence of 100 μM of S-adenosyl-L-methionine (SAM, Solarbio, China) for 1 h at 30°C. Then the reaction was terminated by the addition of 5× SDS–PAGE loading buffer and the samples were resolved by SDS–PAGE. The subsequent steps were the same as Western blot analysis.

Nude mice xenograft tumor model

Four-week-old BALB/c Nude Mice (CAnN.Cg-*Foxn1*^{nu}/Crl), half male and half female, were provided by Vital River (Cat# 401, Beijing, China) and were fed in Specific Pathogen Free (SPF) animal laboratory for animal experiments. All mice were individually numbered and then the random number table was used to group animals. PANC-1 cells (5×10^6 in 100 μl PBS buffer) infected with the indicated lentivirus were injected subcutaneously into the right back of mice after random allocation. The size of heterografts was monitored every 3 days and the volume was calculated with the formula $L \times W^2/2$ (L: length, W: width). After 21 days, all mice were euthanatized to harvest xenografts for photographing and weighing. All animal procedures were approved by the Ethics Committee of Tongji Medical College, Huazhong University of Science and Technology (IACUC number: 2945).

Patient-derived tumor xenograft (PDX) model

Four-week-old NOG Mice (NOD.Cg-*Prkdc*^{scid}*IL2rg*^{tm1Sug}/JicCrl), half male and half female, were provided by Vital River (Cat# 408, Beijing, China) and were fed in Specific Pathogen Free (SPF) animal laboratory for animal experiments. This project involved the collection of pancreatic cancer clinical specimens. The informed consent was obtained from all subjects. The study protocol conformed to the principles of Declaration of Helsinki and was approved by the Medical Ethics Committee of Union Hospital, Tongji Medical College, Huazhong University of Science and Technology (reference number: UHCT-IEC-SOP-016-03-01). Pancreatic cancer tissues were collected sterilely from patients who were undergoing surgical resection for pancreatic cancer at Department of Pancreatic Surgery, Union Hospital, Tongji Medical College, Huazhong University of Science and Technology. Then the cancer tissues were submerged in serum-free DMEM containing 1% Penicillin–Streptomycin and dissected into several small pieces roughly 2 × 2 × 2 mm in size with sterile scalpels and scissors. The NOG mice were anesthetized with isoflurane (Sigma-Aldrich, USA). Next, the small tumor pieces were implanted subcutaneously into the left back of NOG mice (F0 Generation) after being soaked in Matrigel (Corning, USA). When the tumor volume reached approximately 1,500–1,800 mm^3, the xenografts were harvested and implanted subcutaneously into the left back of other NOG mice in the same way (F1 Generation). After F1 Generations grew to a size of 50 mm^3, mice were randomized in the following two groups, with six mice in each group: (1) DMSO (Solarbio, China); (2) GSK3326595 (Selleck, USA) 100 mg/kg every 3 days intravenous injection. The size of xenografts was monitored every 3 days and the volume was calculated with the formula $L \times W^2/2$ (L: length, W: width). After 30 days, all mice were euthanatized for photographing and the xenografts were harvested for photographing, weighing and IHC staining.

Quantification and statistical analysis

GraphPad Prism 8.0 software was used to analyze experimental data and statistical significance. The statistical significance was tested by the unpaired/paired *t*-test or one/two-way analysis of variance (ANOVA). The levels of significance were set at not significant (ns), $P < 0.05$ (*), $P < 0.01$ (**), $P < 0.001$ (***), and it was considered statistically significant as long as $P < 0.05$. The detailed statistical information in every experiment was showed clearly in the figure legends. All statistical results were based on three independent experiments and all values were expressed as mean ± SD.

Data availability

The datasets and computer code produced in this study are available in the following databases: (i) RNA-Seq data: Gene Expression Omnibus GSE241402 (https://www.ncbi.nlm.nih.gov/geo/query/acc.cgi?acc=GSE241402); Reviewer Access Code: ylmdkceinbybvuv. (ii)·Protein interaction AP-MS data: PRIDE PXD044671 (https://proteomecentral.proteomexchange.org/cgi/GetDataset?ID=PXD044671).

Expanded View for this article is available online.

Acknowledgements
We thank the patients and their families for their altruism in participating in research studies. This work was supported by grants from the National Natural Science Foundation of China (grant no. 82073321 to XJ, 82073178 to HW, and 82102789 to DR) and the Natural Science Foundation of Shanxi Province (grant no. 202203021211042 to JM).

Author contributions
Yan Sun: Data curation; writing – original draft. **Xin Jin:** Data curation; validation. **Junpeng Meng:** Resources; methodology. **Feng Guo:** Resources; formal analysis; methodology. **Taoyu Chen:** Resources; methodology. **Xiaoyan Zhao:** Conceptualization; writing – original draft; writing – review and editing. **Heshui Wu:** Conceptualization; funding acquisition; writing – review and editing. **Dianyun Ren:** Conceptualization; data curation; writing – original draft; writing – review and editing.

Disclosure and competing interests statement
The authors declare that they have no conflict of interest.

References

AbuHammad S, Cullinane C, Martin C, Bacolas Z, Ward T, Chen H, Slater A, Ardley K, Kirby L, Chan KT *et al* (2019) Regulation of PRMT5-MDM4 axis is critical in the response to CDK4/6 inhibitors in melanoma. *Proc Natl Acad Sci USA* 116: 17990 – 18000

Ansari D, Ohlsson H, Althini C, Bauden M, Zhou Q, Hu D, Andersson R (2019) The Hippo signaling pathway in pancreatic cancer. *Anticancer Res* 39: 3317 – 3321

Bae SJ, Luo X (2018) Activation mechanisms of the Hippo kinase signaling cascade. *Biosci Rep* 38: BSR20171469

Bae SJ, Ni L, Osinski A, Tomchick DR, Brautigam CA, Luo X (2017) SAV1 promotes Hippo kinase activation through antagonizing the PP2A phosphatase STRIPAK. *Elife* 6: e30278

Bedford MT, Clarke SG (2009) Protein arginine methylation in mammals: who, what, and why. *Mol Cell* 33: 1 – 13

Berglund L, Björling E, Oksvold P, Fagerberg L, Asplund A, Szigyarto CA, Persson A, Ottosson J, Wernérus H, Nilsson P *et al* (2008) A genecentric Human Protein Atlas for expression profiles based on antibodies. *Mol Cell Proteomics* 7: 2019 – 2027

Blanc RS, Richard S (2017) Arginine methylation: the coming of age. *Mol Cell* 65: 8 – 24

Cairns L, Patterson A, Weingartner KA, Koehler TJ, DeAngelis DR, Tripp KW, Bothner B, Kavran JM (2020) Biophysical characterization of SARAH domain-mediated multimerization of Hippo pathway complexes in *Drosophila*. *J Biol Chem* 295: 6202 – 6213

Creasy CL, Ambrose DM, Chernoff J (1996) The Ste20-like protein kinase, Mst1, dimerizes and contains an inhibitory domain. *J Biol Chem* 271: 21049 – 21053

Deng Y, Pang A, Wang JH (2003) Regulation of mammalian STE20-like kinase 2 (MST2) by protein phosphorylation/dephosphorylation and proteolysis. *J Biol Chem* 278: 11760 – 11767

Deng Y, Matsui Y, Zhang Y, Lai ZC (2013) Hippo activation through homodimerization and membrane association for growth inhibition and organ size control. *Dev Biol* 375: 152 – 159

Fan F, He Z, Kong LL, Chen Q, Yuan Q, Zhang S, Ye J, Liu H, Sun X, Geng J *et al* (2016) Pharmacological targeting of kinases MST1 and MST2 augments tissue repair and regeneration. *Sci Transl Med* 8: 352ra108

Fang L, Teng H, Wang Y, Liao G, Weng L, Li Y, Wang X, Jin J, Jiao C, Chen L *et al* (2018) SET1A-mediated mono-methylation at K342 regulates YAP activation by blocking its nuclear export and promotes tumorigenesis. *Cancer Cell* 34: 103 – 118

Fedoriw A, Rajapurkar SR, O'Brien S, Gerhart SV, Mitchell LH, Adams ND, Rioux N, Lingaraj T, Ribich SA, Pappalardi MB *et al* (2019) Anti-tumor activity of the type I PRMT inhibitor, GSK3368715, synergizes with PRMT5 inhibition through MTAP loss. *Cancer Cell* 36: 100 – 114

Ge L, Wang H, Xu X, Zhou Z, He J, Peng W, Du F, Zhang Y, Gong A, Xu M (2020) PRMT5 promotes epithelial-mesenchymal transition via EGFR-β-catenin axis in pancreatic cancer cells. *J Cell Mol Med* 24: 1969 – 1979

Harvey KF, Zhang X, Thomas DM (2013) The Hippo pathway and human cancer. *Nat Rev Cancer* 13: 246 – 257

Hata S, Hirayama J, Kajiho H, Nakagawa K, Hata Y, Katada T, Furutani-Seiki M, Nishina H (2012) A novel acetylation cycle of transcription co-activator Yes-associated protein that is downstream of Hippo pathway is triggered in response to SN2 alkylating agents. *J Biol Chem* 287: 22089 – 22098

Hayashi H, Uemura N, Zhao L, Matsumura K, Sato H, Shiraishi Y, Baba H (2021) Biological significance of YAP/TAZ in pancreatic ductal adenocarcinoma. *Front Oncol* 11: 700315

Hergovich A, Schmitz D, Hemmings BA (2006) The human tumour suppressor LATS1 is activated by human MOB1 at the membrane. *Biochem Biophys Res Commun* 345: 50 – 58

Jin Y, Dong L, Lu Y, Wu W, Hao Q, Zhou Z, Jiang J, Zhao Y, Zhang L (2012) Dimerization and cytoplasmic localization regulate Hippo kinase signaling activity in organ size control. *J Biol Chem* 287: 5784 – 5796

Jin J, Zhang L, Li X, Xu W, Yang S, Song J, Zhang W, Zhan J, Luo J, Zhang H (2022) Oxidative stress-CBP axis modulates MOB1 acetylation and activates the Hippo signaling pathway. *Nucleic Acids Res* 50: 3817 – 3834

Karchugina S, Benton D, Chernoff J (2021) Regulation of MST complexes and activity via SARAH domain modifications. *Biochem Soc Trans* 49: 675 – 683

Kim E, Kang JG, Jho EH, Yang WH, Cho JW (2022) O-GlcNAcylation: an emerging protein modification regulating the Hippo pathway. *Cancer* 14: 3013

Lee MKC, Grimmond SM, McArthur GA, Sheppard KE (2021) PRMT5: an emerging target for pancreatic adenocarcinoma. *Cancer* 13: 5136

Liu L, Zhao X, Zhao L, Li J, Yang H, Zhu Z, Liu J, Huang G (2016) Arginine methylation of SREBP1a via PRMT5 promotes *de novo* lipogenesis and tumor growth. *Cancer Res* 76: 1260 – 1272

Mao W, Mai J, Peng H, Wan J, Sun T (2021) YAP in pancreatic cancer: oncogenic role and therapeutic strategy. *Theranostics* 11: 1753 – 1762

Moroishi T, Hansen CG, Guan KL (2015) The emerging roles of YAP and TAZ in cancer. *Nat Rev Cancer* 15: 73 – 79

Murakami S, Shahbazian D, Surana R, Zhang W, Chen H, Graham GT, White SM, Weiner LM, Yi C (2017) Yes-associated protein mediates immune reprogramming in pancreatic ductal adenocarcinoma. *Oncogene* 36: 1232 – 1244

Murakami S, Nemazanyy I, White SM, Chen H, Nguyen CDK, Graham GT, Saur D, Pende M, Yi C (2019) A Yap-Myc-Sox2-p53 regulatory network dictates metabolic homeostasis and differentiation in Kras-driven pancreatic ductal adenocarcinomas. *Dev Cell* 51: 113 – 128

Neoptolemos JP, Kleeff J, Michl P, Costello E, Greenhalf W, Palmer DH (2018) Therapeutic developments in pancreatic cancer: current and future perspectives. *Nat Rev Gastroenterol Hepatol* 15: 333 – 348

Ni L, Li S, Yu J, Min J, Brautigam CA, Tomchick DR, Pan D, Luo X (2013) Structural basis for autoactivation of human Mst2 kinase and its regulation by RASSF5. *Structure* 21: 1757 – 1768

Praskova M, Khoklatchev A, Ortiz-Vega S, Avruch J (2004) Regulation of the MST1 kinase by autophosphorylation, by the growth inhibitory proteins, RASSF1 and NORE1, and by Ras. *Biochem J* 381: 453 – 462

Praskova M, Xia F, Avruch J (2008) MOBKL1A/MOBKL1B phosphorylation by MST1 and MST2 inhibits cell proliferation. *Curr Biol* 18: 311 – 321

Rawat SJ, Araiza-Olivera D, Arias-Romero LE, Villamar-Cruz O, Prudnikova TY, Roder H, Chernoff J (2016) H-ras inhibits the Hippo pathway by promoting Mst1/Mst2 heterodimerization. *Curr Biol* 26: 1556 – 1563

Sánchez-Sanz G, Tywoniuk B, Matallanas D, Romano D, Nguyen LK, Kholodenko BN, Rosta E, Kolch W, Buchete NV (2016) SARAH domain-mediated MST2-RASSF dimeric interactions. *PLoS Comput Biol* 12: e1005051

Siu LL, Rasco DW, Vinay SP, Romano PM, Menis J, Opdam FL, Heinhuis KM, Egger JL, Gorman S, Parasrampuria R (2019) METEOR-1: a phase I study of GSK3326595, a first-in-class protein arginine methyltransferase 5 (PRMT5) inhibitor, in advanced solid tumours. *Ann Oncol* 30: v159

Stopa N, Krebs JE, Shechter D (2015) The PRMT5 arginine methyltransferase: many roles in development, cancer and beyond. *Cell Mol Life Sci* 72: 2041 – 2059

Thompson BJ (2020) YAP/TAZ: drivers of tumor growth, metastasis, and resistance to therapy. *Bioessays* 42: e1900162

Tran T, Mitra J, Ha T, Kavran JM (2020) Increasing kinase domain proximity promotes MST2 autophosphorylation during Hippo signaling. *J Biol Chem* 295: 16166 – 16179

Villar MV, Spreafico A, Moreno V, Braña I, Hernandez T, Razak AA, Wang J, Haddish-Berhane N, Mehta J, Johnson A (2020) 537MO First-in-human study of JNJ-64619178, a protein arginine methyltransferase 5 (PRMT5) inhibitor, in patients with advanced cancers. *Ann Oncol* 31: S470

Vu LD, Gevaert K, De Smet I (2018) Protein language: post-translational modifications talking to each other. *Trends Plant Sci* 23: 1068 – 1080

Wang YP, Zhou W, Wang J, Huang X, Zuo Y, Wang TS, Gao X, Xu YY, Zou SW, Liu YB *et al* (2016) Arginine methylation of MDH1 by CARM1 inhibits glutamine metabolism and suppresses pancreatic cancer. *Mol Cell* 64: 673 – 687

Wei X, Yang J, Adair SJ, Ozturk H, Kuscu C, Lee KY, Kane WJ, O'Hara PE, Liu D, Demirlenk YM *et al* (2020) Targeted CRISPR screening identifies PRMT5 as synthetic lethality combinatorial target with gemcitabine in pancreatic cancer cells. *Proc Natl Acad Sci USA* 117: 28068 – 28079

Xu J, Richard S (2021) Cellular pathways influenced by protein arginine methylation: implications for cancer. *Mol Cell* 81: 4357 – 4368

Yang Y, Bedford MT (2013) Protein arginine methyltransferases and cancer. *Nat Rev Cancer* 13: 37 – 50

Yin F, Yu J, Zheng Y, Chen Q, Zhang N, Pan D (2013) Spatial organization of Hippo signaling at the plasma membrane mediated by the tumor suppressor Merlin/NF2. *Cell* 154: 1342 – 1355

Yin S, Liu L, Brobbey C, Palanisamy V, Ball LE, Olsen SK, Ostrowski MC, Gan W (2021) PRMT5-mediated arginine methylation activates AKT kinase to govern tumorigenesis. *Nat Commun* 12: 3444

Yu FX, Zhao B, Guan KL (2015) Hippo pathway in organ size control, tissue homeostasis, and cancer. *Cell* 163: 811 – 828

Zheng Y, Pan D (2019) The Hippo signaling pathway in development and disease. *Dev Cell* 50: 264 – 282